Catalysis Science & Technology

Accepted Manuscript

ROYAL SOCIETY OF CHEMISTRY

www.rsc.org/catalysis

Graphic abstract

Rh-Ir-ReO_x/SiO_2 catalyst with ReO_x-modified Ir-Rh alloy particles can convert furfural to 1,5-PeD in high yield.

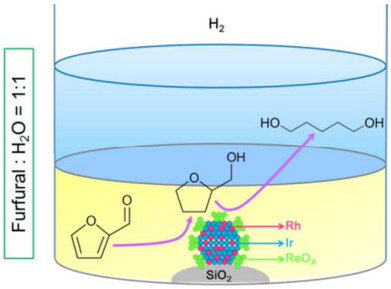

Performance and characterization of rhenium-modified Rh-Ir alloy catalyst for one-pot conversion of furfural into 1,5-pentanediol

Sibao Liu, Yasushi Amada, Masazumi Tamura, Yoshinao Nakagawa* and Keiichi Tomishige*

Department of Applied Chemistry, School of Engineering, Tohoku University, 6-6-07, Aoba, Aramaki, Aoba-ku, Sendai 980-8579, Japan

*Corresponding authors: Keiichi Tomishige and Yoshinao Nakagawa

Department of Applied Chemistry, School of Engineering, Tohoku University

Tel + Fax : +81-22-795-7214

E-mail : tomi@erec.che.tohoku.ac.jp and yoshinao@erec.che.tohoku.ac.jp

Abstract

One-pot selective conversion of highly concentrated furfural to 1,5-pentanediol (1,5-PeD) was carried out over Rh-added Ir-ReO_x/SiO_2 catalysts through two-step reaction temperatures. Over the optimized catalyst, Rh(0.66 wt%)-Ir-ReO_x/SiO_2, the maximum yield of 1,5-PeD was 71.1% from highly concentrated furfural (50 wt%) and 78.2% from diluted furfural (10 wt%). These values were higher than those obtained with Ir-ReO_x/SiO_2 or Pd-Ir-ReO_x/SiO_2 catalysts. Rh-Ir-ReO_x/SiO_2 showed much higher activity in hydrogenation of furfural to tetrahydrofurfuryl alcohol intermediate in the low temperature step than Ir-ReO_x/SiO_2, although the hydrogenation activity was lower than that of Pd-Ir-ReO_x/SiO_2. Long reaction time in the low temperature step is necessary to obtain good 1,5-PeD yield over Rh-Ir-ReO_x/SiO_2 in two-step reaction of furfural. The hydrogenolysis activity of Rh-Ir-ReO_x/SiO_2 for tetrahydrofurfuryl alcohol to 1,5-PeD in the high temperature step was higher than that of Pd-Ir-ReO_x/SiO_2 and was comparable to that of Ir-ReO_x/SiO_2. The characterization results of TPR, XRD, XANES, EXAFS, STEM-EDX and FT-IR of adsorbed CO indicated that Rh-Ir-ReO_x/SiO_2 catalysts showed the structure of Ir-Rh alloy particles partially covered with ReO_x species. The hydrogenation activity of Rh-Ir-ReO_x/SiO_2 for furan ring was higher than those of the mixture of Rh-Ir/SiO_2 and Ir-ReO_x/SiO_2 or the mixture of Rh-ReO_x/SiO_2 and Ir-ReO_x/SiO_2. Both Ir-Rh alloy formation and ReO_x modification of alloy particles are essential for the high hydrogenation activity.

Keywords

hydrogenation, hydrogenolysis, furfural, rhodium, iridium

1. Introduction

The sustainable production of transportation fuels and chemical products from biomass and its derived substrates are attracting more and more attentions since the shortage of fossil resources and an increasing energy demand.[1-8] Furanic compounds are promising intermediates in the production of non-petroleum-derived chemicals for their relatively low oxygen content. Furfural is produced by hydration + dehydration of hemicellulose from agricultural wastes and forest residues on an industrial scale, and it is considered as one of the top 10 chemical opportunities in biorefinery from carbohydrates.[9-12] Selective hydrogenation or total hydrogenation of furfural can give furfuryl alcohol (FFA) and tetrahydrofurfuryl alcohol (THFA)[13-15], which are important building blocks in the synthesis of diols, especially 1,5-pentanediol (1,5-PeD) that can be used as monomers of polyesters and polyurethanes.[16-19] Hydrogenolysis of THFA into 1,5-PeD has been developed using heterogeneous catalysts through multistep or one-step reaction. Schniepp and Geller proposed a multi-step reaction requiring the isolation and purification of intermediates and 70% yield of 1,5-PeD was obtained.[20] Tomishige and coworkers reported one-step hydrogenolysis of THFA into 1,5-PeD using Rh-ReO_x/SiO_2, Rh-MoO_x/SiO_2, Rh-ReO_x/C or Ir-ReO_x/SiO_2 at lower temperature of 373-393 K, 8 MPa.[21-27] The highest yield of 1,5-PeD reached 94%.[23] Dumesic et al.[28] also reported hydrogenolysis of THFA with good performance in the production of 1,5-PeD using Rh-ReO_x/C (Vulcan XC-72). Chatterjee et al.[29] achieved about 73% yield of 1,5-PeD using Rh/MCM-41 in the supercritical CO_2. Also some researchers have paid attention on conversion of furfuryl alcohol into diols. Adkins et al.[30, 31] conducted hydrogenolysis of furfuryl alcohol (FFA) using $CuCr_2O_4$ catalyst at 448 K and 10-15 MPa with high conversion, and 30% of 1,5-PeD and 40% of 1,2-pentanediol (1,2-PeD) were obtained. Although hydrogenolysis of FFA or THFA can give

high yield of 1,5-PeD, the step of hydrogenation of furfural is needed. So, direct conversion of furfural into 1,5-PeD with high activity and selectively is more meaningful. Lu et al.[32] used Pt-Li/Co_2AlO_4 catalyst to convert furfural into 1,5-PeD directly in an alcohol solvent, however the highest yield of 1,5-PeD was only 34.9%. Recently, we reported one-pot conversion furfural into 1,5-PeD over Pd-added Ir-ReO_x/SiO_2 catalyst through two-step temperature reactions and the highest yield of 1,5-PeD is 71.4%.[33] Hydrogenation of furfural to THFA proceeds in lower temperature step and hydrogenolysis of THFA to 1,5-PeD proceeds in higher temperature step. However, the hydrogenolysis activity of Pd-Ir-ReO_x/SiO_2 was lower than Ir-ReO_x/SiO_2.

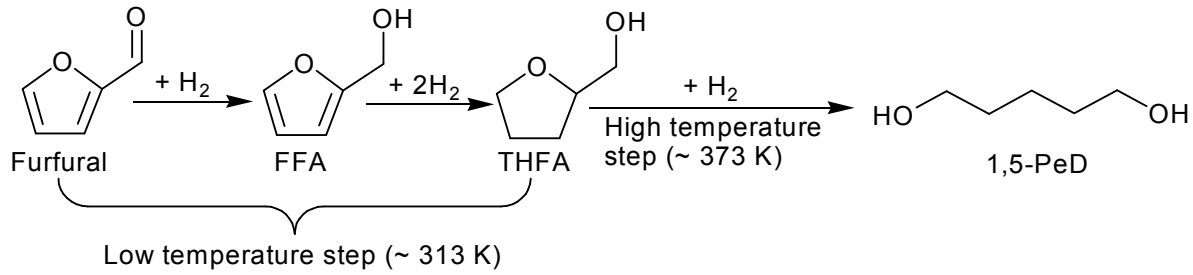

It is known that furfural can be polymerized easily to form humins under high reaction temperature and high concentration of furfural.[34] Rearrangement reactions to 1,4-disubstituted C5 compounds are also well known side-reactions in the reduction of furfural[17,19]. These side reactions remarkably decrease the target 1,5-PeD production. However, conversion of highly concentrated furfural makes large-scale industrial production easier in view of energy consumption. Therefore, conversion of highly concentrated furfural into 1,5-PeD with high yield would shed light on industrial application.

To improve the hydrogenolysis activity and the yield of 1,5-PeD from highly concentrated furfural, in this work, we reinvestigated the additive effect of noble metal to Ir-ReO_x/SiO_2 catalyst for the one-pot aqueous phase conversion of furfural into 1,5-PeD. As a result, it was found that

Rh-Ir-ReO_x/SiO_2 is more effective than Pd-Ir-ReO_x/SiO_2. We also characterized Rh-Ir-ReO_x/SiO_2 with XRD, TPR, XANES, EXAFS, STEM-EDX and FT-IR of adsorbed CO.

2. Experimental

2.1. *Catalyst preparation*

The SiO_2 (G-6, BET surface area 535 m^2/g) supplied by Fuji Silysia Chemical Ltd. was used as a support of the catalysts. Rh-Ir-ReO_x/SiO_2 catalysts were prepared by sequential impregnation method. First, Rh/SiO_2 samples were prepared by impregnating with an aqueous solution of $Rh(NO_3)_3$ (Wako Pure Chemical Industries, Ltd.). After evaporating the solvent and drying at 383 K for 12 h, they were impregnated with an aqueous solution of H_2IrCl_6 (Furuya Metals Co., Ltd). After drying at 383 K for 12 h, the obtained Rh-Ir/SiO_2 samples were impregnated with an aqueous solution of NH_4ReO_4 (Soekawa Chemical Co., Ltd.). These catalysts were calcined in air at 773 K for 3 h after drying at 383 K for 12 h. The loading amounts of Ir and Re were 4.0 and 7.8 wt%, respectively (Re/Ir molar ratio = 2), and the loading amount of Rh is shown in the parenthesis as weight percent: i.e. Rh(0.66)-Ir-ReO_x/SiO_2 contains 0.66 wt% Rh. Pd(0.66)-Ir-ReO_x/SiO_2 catalyst with loading amount of 0.66, 4.0 and 7.8 wt% for Pd, Ir and Re, respectively, was prepared with the same procedure as that reported previously.[33] All the catalysts were used in powdered form with a granule size of <100 mesh.

2.2. *Activity tests*

Activity tests were performed in a 190-ml stainless steel autoclave with an inserted glass vessel. The catalyst was put into an autoclave together with a spinner and an appropriate amount of water and heated at 473 K with 8 MPa H_2 for 1 h for the reduction pretreatment. After the pretreatment, the autoclave was cooled down, and hydrogen was removed. Furfural (Wako Pure Chemical

Industries, Ltd., >95%) was put into the autoclave. The reaction mixture was composed of two layers. The upper layer was furfural-saturated aqueous solution and the bottom layer was furfural. After sealing the reactor, the air content was purged by flushing three times with H_2 (1 MPa, 99.99%; Nippon Peroxide Co., Ltd.). The reactor was pressurized with H_2 to 2.0-10.0 MPa and then heated to set temperature T_1 (303-333 K). The temperature (T_1) was kept for 1-8 h (time 1). After this step (low temperature step), the reaction temperature was increased to another set temperature T_2 (353-413 K). The temperature increase took us about 30 min. The temperature (T_2) was kept for 0-48 h (time 2). These parameters (T_1, time 1, T_2, and time 2) were described for each result. The stirring rate was 500 rpm. After reaction, the reactor was cooled down and the gases were collected in a gas bag. The autoclave contents were transferred to a vial and diluted with the mixture of ethanol and water, and then the catalyst was separated by centrifugation and filtration. The products were analyzed using two kinds of gas chromatographs (Shimadzu GC-2014) equipped with FID. A TC-WAX capillary column (diameter 0.25 mmϕ, 30 m) or an Rtx-1-PONA capillary column (diameter 0.25 mmϕ, 100 m) were used for separation. The products were also identified using GC-MS (QP5050, Shimadzu). The products were furfuryl alcohol (FFA), tetrahydrofurfuryl alcohol (THFA), 1,2,5-pentanetriol (1,2,5-PeT), 1,5-pentanediol (1,5-PeD), 1,4-pentanediol (1,4-PeD), 1,2-pentanediol (1,2-PeD), 1-pentanol (1-PeOH), 2-pentanol (2-PeOH), 2-methyltetrahydrofuran (2-MTHF), *n*-pentane, C-C cracking products (such as methane) and other products that could not be identified ("Others"). The amount of gas products (*n*-pentane and methane) were very small and they were included in "Others". The products were quantified by the external standard method using an aqueous solution of each product with known concentration. The conversion and selectivity were calculated on carbon basis similar to that reported previously.[35]

$$\text{Conversion [\%]} = \frac{\text{mol of furfural after reaction}}{\text{mol of furfural charged}} \times 100$$

$$\text{Yield of products [\%-C]} = \frac{\text{mol}_{\text{product}} \times \text{C atoms in product}}{\text{mol}_{\text{furfural charged}} \times \text{C atoms in furfural}} \times 100$$

$$\text{Yield of unidentified products [\%-C]} = (\text{Conversion} - \text{the sum of yield of products}) \times 100$$

$$\text{TOF(CO)}(h^{-1}) = \frac{\text{product formation rate (mol}\cdot h^{-1})}{\text{adsorption of CO (mol)}}$$

The used catalyst was washed with excess water and dried in air, and then calcined at 573 K or 773 K for 3 h. A slight loss (<8% in weight) was observed during the recovery process and was compensated with fresh catalyst in each reuse experiment. The amount of eluted metal during the reaction was analyzed by inductively coupled plasma atomic emission spectrometry (ICP-AES, Thermo Scientific iCAP 6500).

2.3. *Catalyst characterization*

Temperature-programmed reduction (TPR) was carried out in a fixed-bed reactor equipped with a thermal conductivity detector using 5% H_2 diluted with Ar (30 ml/min). The amount of catalyst was 0.05 g, and the temperature was increased from room temperature to 1123 K at a heating rate of 10 K/min. X-ray diffraction (XRD) patterns were recorded by a diffractometer (Rigaku MiniFlex 600) under air.

The extended X-ray absorption fine structure (EXAFS) spectra were measured at the BL01B1 station at SPring-8 with the approval of the Japan Synchrotron Radiation Research Institute (JASRI; Proposal No. 2013B1037). The storage ring was operated at 8 GeV, and a Si (111) single crystal was used to obtain a monochromatic X-ray beam. Two ion chambers for I_0 and I were filled with 85% N_2+15% Ar and 50% N_2+50% Ar, respectively, for Re L_3-edge and Ir L_3-edge measurements, and 100% Ar and 100% Ar for Rh K-edge measurement. We prepared the samples after the reduction. The reduction process was carried out in an autoclave. The standard reduction conditions

were the same as in activity tests. After cooling, the catalyst powder was transferred to the measurement cell in a glove bag filled with nitrogen. The thickness of the cell filled with the powder was 2 mm to give an edge jump of 1.2, 1.7 and 0.2 for Ir L_3-edge, Re L_3-edge and Rh K-edge measurement, respectively, in the case of Rh-Ir-ReO_x/SiO_2. The EXAFS data were collected in a transmission mode. For EXAFS analysis, the oscillation was first extracted from the EXAFS data using a spline smoothing method.[36] Fourier transformation of the k^3-weighted EXAFS oscillation from the k space to the r space was performed to obtain a radial distribution function. The inversely Fourier filtered data were analyzed using a usual curve fitting method.[37, 38] For curve fitting analysis, the empirical phase shift and amplitude functions for the Re-O, Ir-Ir and Rh-Rh bonds were extracted from data for NH_4ReO_4, Ir powder and Rh foil, respectively. Theoretical functions for the Ir-Rh, Re-Ir, Re-Rh and Rh-Ir bond were calculated using the FEFF8.2 program.[39] The Re-Ir, Ir-Ir and Rh-Ir bonds are represented by the Re-Ir (or -Re), Ir-Ir (or -Re) and Rh-Ir (or -Re), respectively, in the curve fitting results. This is because it is very difficult to distinguish between Ir and Re as a scattering atom. Analyses of EXAFS data were performed using a computer program (REX2000, ver. 2.5.9; Rigaku Corp.). Error bars for each parameter were estimated by stepping each parameter, while optimizing the other parameters, until the residual factor becomes two times as its minimum value.[40]

Transmission electron microscope (TEM) photographs and energy dispersive X-ray (EDX) analysis were taken by means of the instrument (JEM-2010F, JEOL) operated at 200 kV. The sample powders after the reduction were dispersed in 2-propanol by supersonic wave and put on Cu grids for TEM observation under atmosphere.

FT-IR spectra were recorded by a Nicolet 6700 FT-IR with a resolution of 4 cm^{-1} in a diffuse reflectance mode, using an in situ cell (Thermo Spectra-Tech) equipped with a sample cup, heater and ZnSe windows. The powder of catalyst was placed in the sample cup. The cell was connected to the gas flow system. Pretreatment was carried out in H_2 flow at 473 K for 1 h. CO was introduced by pulses with N_2 as a carrier gas at room temperature until the CO coverage reached the saturation level. The FT-IR spectra were collected at room temperature. The amount of CO chemisorption was measured in a high-vacuum system using a volumetric method in the vacuum line. Before adsorption measurements, the catalysts were reduced in H_2 at 473 K for 1 h. Subsequently the adsorption equilibrium, the sample weight and the dead volume of the apparatus was about 1.1 kPa, 0.15 g and 43 cm^3, respectively. Adsorption amount of CO is represented as the molar ratio to Rh (Rh/SiO_2), Ir ($Ir\text{-}ReO_x/SiO_2$) and Ir + Rh ($Rh\text{-}Ir\text{-}ReO_x/SiO_2$).

3. Results and discussion

3.1 Conversion of furfural into 1,5-PeD over different catalysts

In our previous research, catalyst screening was conducted using diluted furfural (10 wt%) and one-step temperature condition at 393 K. [33] At that condition, $Pd\text{-}Ir\text{-}ReO_x/SiO_2$ catalyst showed higher yields of 1,5-PeD than other noble-metal-added $Ir\text{-}ReO_x/SiO_2$ catalysts including $Rh\text{-}Ir\text{-}ReO_x/SiO_2$. However, the highest 1,5-PeD yield was obtained with two-step reaction, 313 K for 8 h and 373 K for 72 h. In this study we re-evaluated the additive effect of noble metal to $Ir\text{-}ReO_x/SiO_2$ using highly concentrated furfural (50 wt%) and two-step reaction (313 K for 8 h and 373 K for 24 h).

First, we investigated the reactions during the low temperature step and the heating to T_2 over various catalysts (Table 1). $Ir\text{-}ReO_x/SiO_2$ catalyst gave FFA very selectively during the low

temperature step (Entry 1).[13] During the heating from T_1 to T_2, the hydrogenation of furan rings didn't proceed over Ir-ReO_x/SiO_2 catalyst (Entry 8), and side-reactions such as polymerization began to start, as reported earlier.[33] On the other hand, both Rh(0.66)-Ir-ReO_x/SiO_2 and Pd(0.66)-Ir-ReO_x/SiO_2 showed good yield of THFA after the low-temperature step (Table 1, Entries 2-3). Compared to Pd(0.66)-Ir-ReO_x/SiO_2 catalyst which has been determined as the best catalyst in the previous study,[33] larger amount of FFA remained over Rh(0.66)-Ir-ReO_x/SiO_2, indicating that Rh(0.66)-Ir-ReO_x/SiO_2 has lower hydrogenation activity. The lower performance of Rh-Ir-ReO_x/SiO_2 than Pd-Ir-ReO_x/SiO_2 in the previous report[33] may be due to the too short reaction time at low temperature in the activity tests for catalyst selection. When heated to 373 K, almost all the FFA was converted into THFA over Rh(0.66)-Ir-ReO_x/SiO_2 (Entry 9). However, the selectivities to other products of Rh(0.66)-Ir-ReO_x/SiO_2 were lower than those of Pd(0.66)-Ir-ReO_x/SiO_2, and the THFA yields were similar for both catalysts (Entry 10). GC-MS analysis suggested that "others" of Entries 2 and 3 contained significant amount of 5-hydroxy-2-pentanone and 1,5-dihydroxy-2-pentanone. These compounds are precursors of 1,4-pentanediol (1,4-PeD) and 1,2,5-pentanetriol (1,2,5-PeT). The physical mixtures of Rh(0.66)/SiO_2 with Ir-ReO_x/SiO_2 showed only 6.6% yield of THFA after the low temperature step (Entry 4). The yield of THFA was still very low even after the reaction temperature reached T_2 (Entry 11). On the other hand, the physical mixtures of Pd(0.66)/SiO_2 with Ir-ReO_x/SiO_2 showed much higher yield of THFA than that of physical mixture of Rh(0.66)/SiO_2 with Ir-ReO_x/SiO_2 (Entries 4,7, 11 and 14). From these results, it could be concluded that the synergistic interaction among Rh, Ir and ReO_x in Rh(0.66)-Ir-ReO_x/SiO_2 enhanced the hydrogenation rate of furan ring.

The reaction results after high temperature step are listed in Table 2. Rh(0.66)-Ir-ReO_x/SiO_2 catalyst showed higher 1,5-PeD yield than Pd(0.66)-Ir-ReO_x/SiO_2 (Entry 5). Different Rh loading amount (Entries 1-8) were tested. The best performance was obtained when Rh loading amount was 0.66 wt%. In these conditions, over Pd(0.66)-Ir-ReO_x/SiO_2 catalyst significant amount of THFA intermediate remained in the reaction mixtures (Entry 9). When reaction time was prolonged to 48 h, the yield of 1,5-PeD over Pd(0.66)-Ir-ReO_x/SiO_2 catalyst was still lower than that over Rh(0.66)-Ir-ReO_x/SiO_2 catalyst and larger amount of 1-pentanol was formed (Entry 10). The physical mixture of Rh(0.66)/SiO_2 and Ir-ReO_x/SiO_2 showed only 2.1% of 1,5-PeD (Entry 11) while the mixture of Pd(0.66)/SiO_2 and Ir-ReO_x/SiO_2 showed 35.0% yield of 1,5-PeD (Entry 12). Compared to Pd(0.66)-Ir-ReO_x/SiO_2, the synergistic interaction among Rh, Ir and ReO_x in Rh(0.66)-Ir-ReO_x/SiO_2 was more obvious.

The catalysts were prepared with sequential impregnation method, and drying at 383 K was conducted between the impregnation steps. We also prepared Rh(0.66)-Ir-ReO_x/SiO_2 samples with different preparation procedures: (A) successive impregnation with calcination after each drying process and (B) co-impregnation. However, the activity tests showed that both of samples A and B had lower hydrogenation activity than the catalyst prepared by standard method (Table S1). It should be noted that black precipitate was formed when the three precursors were mixed together in water. Preparation by these procedures ((A) or (B)) was unsuitable to develop the synergistic interaction.

Conversion of diluted furfural (10 wt%) was also conducted over Rh(0.66)-Ir-ReO_x/SiO_2 and Pd(0.66)-Ir-ReO_x/SiO_2 catalysts. The yields of 1,5-PeD over both Rh(0.66)- and Pd(0.66)-Ir-ReO_x/SiO_2 catalysts were higher and those of unidentified products were lower than in

the case of highly concentrated furfural, for the intrinsic polymerization property of highly concentrated furfural (Entries 15 and 17). After 24 h high-temperature step reaction, the yield of 1,5-PeD over Rh(0.66)-Ir-ReO_x/SiO_2 was higher than that over Pd(0.66)-Ir-ReO_x/SiO_2 (Entries 15 and 17). When the reaction time was prolonged to 32 h, the highest yield of 1,5-PeD over Rh(0.66)-Ir-ReO_x/SiO_2 reached 78.2% in the low concentration of furfural conversion (Entry 16). This value was higher than the maximum yield over Pd(0.66)-Ir-ReO_x/SiO_2 catalyst (71.4%). In addition, the reaction time is much shorter than the time required to obtain the highest yield over Pd(0.66)-Ir-ReO_x/SiO_2 (72 h).

Fig. 1 shows the effect of reaction times on the conversion of furfural over Rh(0.66)- and Pd(0.66)-Ir-ReO_x/SiO_2 catalysts. For simplicity, the yields of the main products such as FFA, THFA, 1,2,5-PeT and 1,5-PeD are displayed. The data in detail are shown in Tables S2 and S3 (ESI). In the low-temperature step, almost all the furfural was converted over both Rh(0.66)- and Pd(0.66)-Ir-ReO_x/SiO_2 catalysts in 1 h, and the main products were FFA and THFA. As time going, FFA was further hydrogenated into THFA, indicating that the formation of THFA originated from furfural via selective hydrogenation of furfural into FFA and subsequent hydrogenation of furan rings. The rate of hydrogenation of furan ring as determined by the slope of THFA yield during 1-3 h was higher over Pd(0.66)-Ir-ReO_x/SiO_2 than that over Rh(0.66)-Ir-ReO_x/SiO_2. The high activity of Pd-added catalyst may be due to the strong interaction between the Pd metal and π electrons of the FFA molecule resulting from rehybridization of sp^2 to sp^3 of C on the Pd surface.[41] The yield of 1,2,5-PeT increased as reaction time was prolonged. The production of 1,2,5-PeT originates from FFA by ring-opening acid hydrolysis reaction and subsequent hydrogenation.[42] The hydrogenation reaction was almost complete over Pd(0.66)-Ir-ReO_x/SiO_2 catalyst after 8 h, and when heating to

373 K, the product distributions were almost the same over Pd(0.66)-Ir-ReO_x/SiO_2. In the case of Rh(0.66)-Ir-ReO_x/SiO_2, hydrogenation of FFA was not complete after 8 h. However, it proceeded quickly during the heating to T_2. At high-temperature step, 1,5-PeD began to be produced over both catalysts. As reaction time going, the yield of 1,5-PeD increased gradually while THFA and 1,2,5-PeT decreased, suggesting that both THFA and 1,2,5-PeT were the intermediates of 1,5-PeD. Based on reaction time 4 h (as time 2), the formation rate of 1,5-PeD over Rh(0.66)-Ir-ReO_x/SiO_2 catalyst was 2.3 times higher than that of Pd(0.66)-Ir-ReO_x/SiO_2 catalyst. The difference was even larger in TOF(CO) values (190 h^{-1}/57 h^{-1}). These data indicate the higher hydrogenolysis activity of Rh(0.66)-Ir-ReO_x/SiO_2 catalyst. To compare the hydrogenolysis activity of these catalysts more clearly, catalytic tests using 50 wt% THFA as reactant were also conducted (Table 3). Indeed, the hydrogenolysis activity of Rh(0.66)-Ir-ReO_x/SiO_2 was higher than that of Pd(0.66)-Ir-ReO_x/SiO_2 and it was comparable to that of Ir-ReO_x/SiO_2. The selectivities to 1,5-PeD were very high for all of these three catalysts and no 1,2,5-PeT was formed over all the catalysts. Therefore, higher performance of Rh(0.66)-Ir-ReO_x/SiO_2 is originated from high selectivity in the hydrogenation of furfural and high activity in the hydrogenolysis reaction. Formation of 1,2,5-PeT intermediate was probably due to the hydrolysis and hydrogenation of FFA. The possible reaction routes was shown in Scheme 1.

3.2 Effect of reaction conditions

Table 4 shows the effect of reaction temperature on production of 1,5-PeD from furfural over Rh(0.66)-Ir-ReO_x/SiO_2 under 6 MPa of hydrogen. After low temperature step, the yield of THFA increased as T_1 increased from 303 K to 323 K and the yield decreased at 333 K (Entries 1-4). At T_1 = 333 K, the selectivity to "Others" was very high and the colour of solution was pale yellow, while

at lower T_1 the solutions were almost colourless. This suggests that polymerization of furfural proceeded at high T_1. After high temperature step, the yield of 1,5-PeD was lower and that of 1,4-PeD and 1,2,5-PeT was higher when higher T_1 was applied (Entries 5-8). This indicated that high T_1 leads rearrangement side reaction to 1,4-PeD[19] and hydrolysis + hydrogenation reaction to 1,2,5-PeT[42]. In addition, as T_1 increased, yield of unidentified products increased even after high temperature step. Therefore, lower T_1 was more preferred to the production of 1,5-PeD. As the temperature of high-temperature step (T_2) increased from 353 K to 413 K, the yield of 1,5-PeD showed a volcano-type performance and that of THFA and 1,2,5-PeT, which are the intermediates of 1,5-PeD, decreased gradually (Entries 9-12). The overhydrogenolysis product 1-pentanol increased quickly as reaction temperature increased. As a result, 373 K was optimum. It should be noted that the yield of 1-pentanol reached 34.6% when reaction temperature was 413 K while 1-pentanol is very attractive for gasoline components for its moderate vapor pressure and low water solubility.[43]

Table 5 shows the effect of hydrogen pressure on conversion of furfural over Rh(0.66)-Ir-ReO_x/SiO_2. A large increases in the 1,5-PeD yield and conversions of THFA and 1,2,5-PeT occurred when the H_2 pressure was elevated from 2 to 8 MPa, in consistent with the first-order dependence of hydrogenolysis rate over Ir-ReO_x/SiO_2.[27] The highest yield of 1,5-PeD was 71.1% when the pressure was 8 MPa (Entry 4). The yield of unidentified products decreased sharply as H_2 pressure increased. This is probably because low H_2 pressure decreases the hydrogenation rate of furfural to THFA, and reaction time of low temperature step becomes too short. However, hydrogen pressure increased further to 10 MPa, the yield of 1,5-PeD decreased

slightly and the overhydrogenolysis product 1-pentanol increased with an increase in pressure (Entry 5).

3.3 Catalyst stability

Table 6 lists the results of the activity test of the reused Rh(0.66)-Ir-ReO_x/SiO_2. The method of the catalyst reuse was as follows: the catalyst was washed with water and dried at 383 K for 12 h and calcined in air at 573 K or 773 K for 3 h. Before the activity test, the reduction pretreatment was carried out in the same way for the fresh catalyst. First, the used catalyst was calcined at 773 K, similarly to the cases with Ir-ReO_x/SiO_2[44,45] or Pd-Ir-ReO_x/SiO_2[33]. The 1,5-PeD yield was decreased with reuses in both cases for concentrated and diluted furfural. This is contrast to the case of Pd-Ir-ReO_x/SiO_2 that showed similar activity after reuses.[33] To identify the cause of the catalyst deactivation, Inductively coupled plasma (ICP) and XRD characterizations were conducted. ICP analysis of the reaction solution after the catalyst had been removed by filtration showed no leaching of Ir and Rh (below detection limit) and slight leaching of Re (0.8-2.8% for each run, Table 6). The XRD peaks (Fig. S1, ESI) of the catalysts after the 3rd run became sharper than those of the catalysts after reduction and the 1st reaction, indicating the aggregation of metal during regeneration. The aggregation could be the reason for the decrease in the 1,5-PeD formation. We further conducted the reuse test with low calcination temperature (573 K) during regeneration process in order to suppress aggregation. However, the 1,5-PeD yield was more significantly decreased (Table 6). The XRD pattern of reused catalyst showed aggregation similarly to the case with 773 K calcination (Fig. S1). Therefore, Rh-Ir-ReO_x/SiO_2 catalyst more easily aggregates than Ir-ReO_x/SiO_2 and Pd-Ir-ReO_x/SiO_2, resulting lower stability. The more rapid deactivation of used catalyst after

573 K calcination may be due to formation of carbonaceous deposit which can be removed by calcination at higher temperature.

3.4 Catalyst characterization

The profiles of temperature-programmed reduction (TPR) of Rh-Ir-ReO_x/SiO_2, Ir-ReO_x/SiO_2, Rh-ReO_x/SiO_2, ReO_x/SiO_2, Ir/SiO_2 and Rh/SiO_2 after calcination are shown in Fig. 2 and the results including the consumption of H_2 and the calculated valence of Re are listed in Table 7. In the case of the monometallic catalysts, Rh/SiO_2 was reduced at very low temperature (Fig. 2a). Ir/SiO_2 was completely reduced at 600 K (Fig. 2b) while ReO_x/SiO_2 was partially reduced at 800 K to the valence of +1.6 (Fig. 2c).[44] In the cases of the bimetallic catalysts, Ir-ReO_x/SiO_2 showed only one large peak centered at around 460 K (Fig. 2f).[44, 45] Rh-ReO_x/SiO_2 showed two peaks between 365 K and 436 K (Fig. 2e). Rh-Ir/SiO_2 showed one broad peak at temperature range between Rh/SiO_2 and Ir/SiO_2 (Fig. 2d). In the case of trimetallic catalysts, Rh-Ir-ReO_x/SiO_2 showed only one broad signal when loading amount of Rh was below 1 wt%. The reduction temperature range was lower than Ir-ReO_x/SiO_2 indicating the presence of Rh promoted the reduction of Ir-ReO_x/SiO_2. In the case of the catalysts with loading amount of Rh $\leq$ 0.5 wt%, the H_2 consumption signal was shifted to low temperature range with increasing Rh amount (Fig 2g-i). The reduction temperature was almost unchanged by more Rh addition (Fig. 2j-l). When the loading amount of Rh was 2 wt%, three signals appeared (Fig. 2m). The two signals at lower temperature may be assigned to Rh-ReO_x/SiO_2 reduction, suggesting that Ir-free Rh-ReO_x species existed on Rh(2)-Ir-ReO_x/SiO_2 catalyst. The peak areas in the profiles of Ir-ReO_x/SiO_2 and Rh-Ir-ReO_x/SiO_2 corresponded to the reduction of Re species to the valence of 2-5 in addition to the total reduction of Ir and Rh. The valence of Re in Rh-Ir-ReO_x/SiO_2 was lower than that of Ir-ReO_x/SiO_2, demonstrating that the addition of Rh

promoted the reduction of Re species (Table 8). The valence of Re species after reduction was also determined by Re L_3-edge XANES (3.1 for Ir-ReO_x/SiO_2 and 2.3-2.4 for Rh-Ir-ReO_x/SiO_2). Similarly to TPR results, the valence of Re in Rh-Ir-ReO_x/SiO_2 was lower than that of Ir-ReO_x/SiO_2. The difference in the valence from the XANES analysis and TPR can be explained by the difference of pretreatment conditions between P_{H2} = 8 MPa in water in XANES/EXAFS measurement and P_{H2} = 0.05 atm in N_2 flow in TPR. Similar tendency in the valence difference was also observed in the cases of Ir-ReO_x/SiO_2 [44-46], Rh-ReO_x/SiO_2[47] and Pt-ReO_x/SiO_2.[48, 49] The spectra and the detailed analysis of Re L_3-edge XANES are shown in Fig. 3. We have reported that the Re L_3-edge XANES analysis of Pd-Ir-ReO_x/SiO_2, and the valence of Re was determined to be 3.1. The activity trend of these catalysts (Table 3); Ir-ReO_x/SiO_2 > Rh-Ir-ReO_x/SiO_2 > Rh-Ir-ReO_x/SiO_2 for hydrogenolysis is different from the order of the valence of Re.

Figure 4 shows XRD patterns of Rh-Ir-ReO_x/SiO_2 after reaction and Ir-ReO_x/SiO_2, Rh-ReO_x/SiO_2, Rh-Ir/SiO_2, ReO_x/SiO_2, Ir/SiO_2 and Rh/SiO_2 after reduction with 8 MPa H_2 at 473 K for 1 h. In the cases of monometallic catalysts, Ir/SiO_2 showed the peaks at 2θ = 41.3°, 47.3° and 69.1° which were assigned to Ir metal.[50] Rh/SiO_2 showed no diffraction peaks, because of low Rh amount and / or the high dispersion. ReO_x/SiO_2 showed small peaks at 2θ = 37.5°, 40.5° and 42.9° which were assigned to Re metal[51]. It should be noted that most Re species were in the oxidized state based on the TPR and XANES results. In the cases of bimetallic catalysts, Rh-ReO_x/SiO_2 also showed no peaks, suggesting that Rh and Re species were highly dispersed. Rh-Ir/SiO_2 exhibited the pattern which was similar to Ir/SiO_2 catalyst but the peak of metal (111) was shifted to smaller angle indicating the formation of Rh-Ir alloy. Ir-ReO_x/SiO_2 showed the pattern whose peak positions were almost the same as those of Ir/SiO_2 while the peaks were broadened by the addition of Re, as reported earlier.[44]

The peaks corresponding to Re metal or ReO_x were not detected at all. These results indicate that Ir metal and highly dispersed Re species are present and the average metal particle size of Ir was decreased by addition of Re[44]. In the case of Rh-added Ir-ReO_x/SiO_2 catalysts, the XRD patterns of Rh-Ir-ReO_x/SiO_2 were similar to that of Ir-ReO_x/SiO_2 and the peak of metal (111) plane (around 41°) was shifted to smaller angle gradually with the increasing Rh amount, especially ≥ 1 wt% (Fig. 4B), from 41.3 ° (Ir-ReO_x/SiO_2) to 41.0 ° (Rh(2)-Ir-ReO_x/SiO_2), suggesting that Rh-Ir alloy was formed.

Further characterization of Rh-Ir-ReO_x/SiO_2 catalysts were carried out using Ir L_3-edge, Re L_3 edge and Rh *K*-edge EXAFS (Tables 8-10) and the detailed spectra and analyses are shown in Figs. 5-7. The Ir L_3-edge curve fitting results of Rh-Ir-ReO_x/SiO_2 after reduction were different from that of Ir-ReO_x/SiO_2, and this can be explained by the presence of the Ir-Rh bond, which suggests the interaction between Ir and Rh. If the curve fittings were carried out without Ir-Rh bond, the fitting was much worse than that with Ir-Rh bond (Table S4 and Fig. S2, ESI), which strongly supported the existence of Ir-Rh bond. The bond distance of the Ir-Rh bond is about 0.271-0.272 nm, which lies between the Ir-Ir bond (0.276 nm) and Rh-Rh (0.268 nm). At the same time, Ir-Ir bond distance on Rh-Ir-ReO_x/SiO_2 catalysts is almost as same as that in Ir-ReO_x/SiO_2 metal. The behavior of these bond lengths suggests the formation of Ir-Rh alloy with predominantly metallic Ir. The coordination number (CN) of the Ir-Rh bond increased and the CN of the Ir-Ir bond decreased with increasing Rh amount. However, the sum of coordination number (CN) of Ir-Rh and Ir-Ir in Rh-Ir-ReO_x/SiO_2 was 10.7-10.9 which is comparable to that of Ir-ReO_x/SiO_2, suggesting that Ir-Rh alloy particle size of Rh-Ir-ReO_x/SiO_2 is almost the same as that of Ir-ReO_x/SiO_2 which was determined to be 1.9 nm.[44]

Fig. 6 shows the Re L_3-edge EXAFS spectra of Ir-ReO_x/SiO_2 after catalytic use and Rh-Ir-ReO_x/SiO_2 after reduction. Table 9 listed the curve fitting results. The curve fitting analysis

indicated the presence of the Re-O, Re-Ir (or -Re) in all of the samples, with bond length (*R*) of 0.203-0.205 and 0.266-0.267 nm, respectively, and CN of 1.0-1.7 and 5.3-6.1, respectively. The presence of the Re-O bond indicates that Re species is not fully reduced to the metallic state and this is supported by TPR and Re L_3-edge XANES analysis. Although the Re-Rh bond on Rh(0.66)-Ir-ReO_x/SiO_2 was not detected, both Rh(1)-Ir-ReO_x/SiO_2 and Rh(2)-Ir-ReO_x/SiO_2 showed Re-Rh bond and the CN increased with the increasing Rh amount, indicating that the interaction between ReO_x species and Rh species exists. If the curve fitting was carried out without Re-Rh bond, the fitting was much worse than that with Re-Rh bond (Table S5 and Fig. S3, ESI), which strongly supported the existence of Re-Rh bond. The CN of the Re-Ir (or -Re) bonds decreased with increasing Rh content, which is explained by the increase in CN of the Re-Rh bond.

The Rh *K*-edge EXAFS curve fitting analysis of Rh-Ir-ReO_x/SiO_2 showed that Rh was in metallic state (Table 10 and Fig. 7). The presence of both the Rh-Rh bond and Rh-Re (or -Ir) bond was verified. The CN of the Rh-Rh bond increased with increasing Rh content. If the curve fitting was carried out without Rh-Rh bond, the fitting was much worse than that with Rh-Rh bond (Table S6 and Fig. S4, Supplementary data), which strongly supported the existence of Rh-Rh bond. The coordination number of the Rh-Ir bond and Rh-Rh bond in Rh *K*-edge EXAFS gives the information on the miscibility. In the homogenously mixed alloy, the ratio (relative to the Rh atom) of the coordination number $CN_{Rh\text{-}Ir}$ to $CN_{Rh\text{-}Rh}$ is equal to the mole fraction ratio n_{Ir}/n_{Rh} of the elements in the bulk, i.e. $CN_{Rh\text{-}Ir}/CN_{Rh\text{-}Rh} = n_{Ir}/n_{Rh}$[52]. In the case of Rh-Ir-ReO_x/SiO_2, it is difficult to determine $CN_{Rh\text{-}Ir}$ directly from the result of Rh *K*-edge EXAFS analysis, because the contribution of Ir and Re as a backscattering atom is not distinguishable. Therefore, $CN_{Rh\text{-}Ir}$ was determined by using the relationship of $CN_{Rh\text{-}Ir} = n_{Ir}/n_{Rh} \times CN_{Ir\text{-}Rh}$. As a result, $CN_{Rh\text{-}Ir}$ is calculated to be 7.2, 5.0 and 2.8 for

Rh(0.66)-, Rh(1)- and Rh(2)- Ir-ReO_x/SiO_2, respectively. In the case of Rh(0.66)- and Rh(1)-Ir-ReO_x/SiO_2, the ratio of coordination number CN_{Rh-Ir}/CN_{Rh-Rh} are 3.6 and 1.8, respectively, which are almost the same as the actual mole fraction ratio n_{Ir}/n_{Rh} 3.3 and 2.1, respectively. This finding indicates that metallic Rh atoms can be mixed well with Ir atoms. However, in the case of Rh(2)-Ir-ReO_x/SiO_2, the ratio of coordination number CN_{Rh-Ir}/CN_{Rh-Rh} are 0.6 which is much lower than the actual mole fraction ratio n_{Ir}/n_{Rh} 1.1, indicating that the miscibility of Ir-Rh alloy was low. There are two possible structures of Rh(2)-Ir-ReO_x/SiO_2 to explain the low miscibility of Ir-Rh alloy. The first one is that Rh metal particles can be partially formed without the interaction with Ir-Rh alloy. The other one is that the surface segregation of Rh species in the Ir-Rh alloy particles. On the other hand, TPR profiles gave three signals which is analogous to Pd-Ir-ReO_x/SiO_2 which has been reported before[33], suggesting that Ir-free Rh metal particles modified with ReO_x species existed on Rh(2)-Ir-ReO_x/SiO_2 catalyst.

Based on the above results on the structural analysis, Rh(0.66)- and Rh(1)-Ir-ReO_x/SiO_2 catalyst has the structure that Ir-Rh alloy formed and ReO_x species are located on Ir-Rh metals. The miscibility of Ir-Rh alloy was well. On Rh(2)-Ir-ReO_x/SiO_2 catalysts, both Ir-Rh alloy partially covered with ReO_x species and small Rh metal particles also partially covered with ReO_x species existed on SiO_2 support. This property is unique for the case of Rh addition, judging from no alloy formation in the case of Pd and Ru addition.[33, 53]

STEM-EDX analysis with element mapping of the Rh(0.66)-Ir-ReO_x/SiO_2 catalyst was conducted to investigate the distribution of the metallic nanoparticles on the silica (Fig. 8). Fig. 8b and c showed the image of the silica support. The distribution of Si is similar to that of O. The blue area in the image of Fig. 8d is of the Ir metal phase. The green one of Fig. 8e is attributed to Rh metal

species, and the green area well overlapped the blue one. It is highly likely that the two metals formed alloy in the catalyst. For Re (Fig. 8f), it is difficult to determine the dispersion because ReO_x can be easily oxidized during the preparation of TEM-EDX samples. The image suggested higher concentration of Re on the metal particles. The Re intensity on the support might be due to the oxidized species.

The FT-IR spectra of adsorbed CO on the in situ reduced catalysts at room temperature are given in Fig. 9. The IR spectrum of Rh(0.66)/SiO_2 interacting with CO at room temperature exhibited a strong band at 2072 cm^{-1}, which can be attributed to linear adsorbed CO; a doublet at 2092 cm^{-1} and 2034 cm^{-1}, which can be assigned to the symmetric and asymmetric carbonyl stretching frequencies of gem-dicarbonyl Rh(I)$(CO)_2$; and a broad peak at 1865 cm^{-1}, which is assigned to bridge-bonded CO.[54] The formation of the dicarbonyl species could be an indication of highly dispersed Rh since it is widely accepted that the dicarbonyl species can only be formed on highly dispersed rhodium.[55, 56] All of the Rh-Ir-ReO_x/SiO_2 didn't show the peak assigned to the bridge CO adsorption on Rh metal surface, but showed similar spectral patterns to that of Ir-ReO_x/SiO_2 with broader absorption band indicating that Rh was in metallic state. The position of the peak top was located between 2066 and 2069 cm^{-1} which can be assigned to the linear CO adsorbed on Ir-Rh alloy surface. In addition, metal Rh is also partially covered with the low-valent ReO_x species which could not adsorb CO. In the case of Rh(2)-Ir-ReO_x/SiO_2, a small adsorption band at 2099 cm^{-1} appeared. This peak is assigned to the symmetric carbonyl stretching frequencies of gem-dicarbonyl Rh(I)$(CO)_2$, indicating that some Rh metal particles with smaller size existed on Rh(2)-Ir-ReO_x/SiO_2 catalyst.

According to the catalytic performance and the proposed catalyst model, the formation of Ir-Rh alloy partially covered with ReO_x species on Rh(0.66)-Ir-ReO_x/SiO_2 catalysts played an important

role in catalytic performance. The physical mixture of Rh(0.66)-Ir/SiO_2 and Ir-ReO_x/SiO_2 catalysts showed higher yield of THFA in the low temperature step than the physical mixture of Rh(0.66)/SiO_2 and Ir-ReO_x/SiO_2 catalysts or the physical mixture of Rh(0.66)-ReO_x/SiO_2 and Ir-ReO_x/SiO_2 catalysts, indicating that Ir-Rh alloy enhanced the hydrogenation activity of furan rings (Table 1, Entries 4-6 and 11-13). However, the yield of THFA was still much lower than that of Rh(0.66)-Ir-ReO_x/SiO_2 (Table 1, Entries 2, 5, 9 and 13). The yield of target product 1,5-PeD in two-step reaction (Table 2, Entries 5 and 13) was also lower. The CO adsorption amount of Rh(0.66)-Ir-ReO_x/SiO_2 (0.020 mmol) was similar to that of these mixed catalysts (0.022, 0.021 and 0.022 mmol for Rh(0.66)-Ir/SiO_2 + Ir-ReO_x/SiO_2, Rh(0.66)/SiO_2 + Ir-ReO_x/SiO_2 and Rh(0.66)-ReO_x/SiO_2 + Ir-ReO_x/SiO_2, respectively). Therefore, high performance of Rh(0.66)-Ir-ReO_x/SiO_2 will be due to the Ir-Rh alloy modified with ReO_x species. This unique structure improves the total hydrogenation performance in low temperature step which is the key step for the production of 1,5-PeD. It should be noted that Rh catalysts modified with metal oxide such as ReO_x have high activity in THFA hydrogenolysis, similarly to Ir-ReO_x/SiO_2 catalyst[21, 27]. On the other hand, Pd has almost no activity in THFA hydrogenolysis. Higher hydrogenolysis activity of Rh-Ir-ReO_x/SiO_2 than Pd-Ir-ReO_x/SiO_2 may be due to the difference of intrinsic activity between Rh and Pd.

4. Conclusions

In one-pot two-step temperature reaction, addition of Rh to Ir-ReO_x/SiO_2 catalyst (Rh-Ir-ReO_x/SiO_2) gave higher yield of 1,5-PeD from furfural in shorter total reaction time than the addition of Pd (Pd-Ir-ReO_x/SiO_2). Rh(0.66)-Ir-ReO_x/SiO_2 showed higher activity for hydrogenolysis of tetrahydrofurfuryl alcohol intermediate to 1,5-PeD than Pd(0.66)-Ir-ReO_x/SiO_2 and the activity was

comparable to that of Ir-ReO_x/SiO_2. For the total hydrogenation of furfural to tetrahydrofurfrual alcohol, Rh(0.66)-Ir-ReO_x/SiO_2 has lower activity, but lower selectivity to undesirable side products than Pd(0.66)-Ir-ReO_x/SiO_2. The highest yield of 1,5-PeD was 71.1% from highly concentrated furfural (50 wt%) and 78.2% from diluted furfural (10 wt%) when using Rh (0.66 wt%)-Ir-ReO_x/SiO_2 as catalyst. The lower performance of Rh-Ir-ReO_x/SiO_2 than Pd-Ir-ReO_x/SiO_2 in the previous report[33] may be due to the too short reaction time for hydrogenation (at low temperature) in the activity tests. In view of stability, Rh-Ir-ReO_x/SiO_2 catalyst can aggregate more easily than Pd-Ir-ReO_x/SiO_2.

Characterizations of TPR, XRD, XANES, EXAFS STEM-EDX and FT-IR of adsorbed CO were performed. The results indicated that Rh(0.66)- and Rh(1)-Ir-ReO_x/SiO_2 catalyst has the structure of Ir-Rh alloy partially covered with ReO_x species. However, besides ReO_x-species-modified Ir-Rh alloy, small size Rh particles modified with ReO_x species also existed on Rh(2)-Ir-ReO_x/SiO_2 catalysts.

High performance of Rh(0.66)-Ir-ReO_x/SiO_2 could be attributed to its unique structure. The ReO_x-species-modified Ir-Rh alloy enhanced the hydrogenation rate of furfural into tetrahydrofurfuryl alcohol (THFA) intermediate in the low temperature step as compared to Ir-ReO_x/SiO_2. THFA was converted to 1,5-pentandiol by hydrogenolysis during the high temperature step over the same ReO_x-modified Ir-Rh alloy.

Acknowledgements

This work was in part supported by the Cabinet Office, Government of Japan through it's "Funding Program for Next Generation World-Leading Researchers". Sibao Liu thanks the China Scholarship

Council (CSC) for the financial support. Authors appreciate Dr. Ya Xu for STEM-EDX observation of the catalyst.

References

[1] G. W. Huber, S. Iborra and A. Corma, *Chem. Rev.*, 2006, **106**, 4044-4098.
[2] J.C. Serrano-Ruiz, R. Luque and A. Sepulveda-Escribano, *Chem. Soc. Rev.*, 2011, **40**, 5266-5281.
[3] P. Gallezot, *Chem. Soc. Rev.*, 2012, **41**, 1538-1558.
[4] M. Schlaf, *Dalton Trans.*, 2006, 4645-4653.
[5] H. Kobayashi and A. Fukuoka, *Green. Chem.*, 2013, **15**, 1740-1763.
[6] A. Corma, S. Iborra and A. Velty, *Chem. Rev.*, 2007, **107**, 2411-2502.
[7] A. M. Ruppert, K. Weinberg and R. Palkovits, *Angew. Chem. Int. Ed.*, 2012, **51**, 2564-2602.
[8] M. Yabushita, H. Kobayashi and A. Fukuoka, *Appl. Catal. B: Environ.*, 2014, **145**, 1-9.
[9] J. J. Bozell and G. R. Petersen, *Green. Chem.*, 2010, **12**, 539-554.
[10] A. S. Mamman, J. M. Lee, Y. C. Kim, I. T. Hwang, N. J. Park, Y. K. Hwang, J. S. Chang and J. S. Hwang, *Biofuels Bioprod. Biorefin.*, 2008, **2**, 438-454.
[11] R. Xing, A. V. Subrahmanyam, H. Olcay, W. Qi, G. P. van Walsum, H. Pendse and G. W. Huber, *Green Chem.*, 2010, **12**, 1933-1946.
[12] R. Weingarten, G. A. Tompsett, W. C. Conner and G. W. Huber, *J. Catal.*, 2011, **279**, 174-182.
[13] M. Tamura, K. Tokonami, Y. Nakagawa and K. Tomishige, *Chem. Commun.*, 2013, **49**, 7034-7036
[14] Y. Nakagawa and K. Tomishige, *Catal. Commun.*, 2010, **12**, 154-156.
[15] Y. Nakagawa, H. Nakazawa, H. Watanabe and K. Tomishige, *ChemCatChem*, 2012, **4**, 1791-1797.
[16] Y. Nakagawa and K. Tomishige, *Catal. Surv. Asia*, 2011, **15**, 111-116.
[17] J. P. Lange, E. van der Heide, J. van Buijtenen and R. Price, *ChemSusChem*, 2012, **5**, 150–166.
[18] Y. Nakagawa and K. Tomishige, *Catal. Today*, 2012, **195**, 136-143.
[19] Y. Nakagawa, M. Tamura and K. Tomishige, *ACS Catal.*, 2013, **3**, 2655-2668.
[20] L.E. Schniepp and H.H. Geller, *J. Am. Chem. Soc.*, 1946, **68**, 1646-1648.
[21] S. Koso, I. Furikado, A. Shimao, T. Miyazawa, K. Kunimori and K. Tomishige, *Chem. Commun.*, 2009, 2035–2037.
[22]S. Koso, N. Ueda, Y. Shinmi, K. Okumura, T. Kizuka and K. Tomishige, *J. Catal.*, 2009, **267**, 89–92.
[23] K. Y. Chen, S. Koso, T. Kubota, Y. Nakagawa and K. Tomishige, *ChemCatChem*, 2010, **2**, 547-555.
[24] S. Koso, Y. Nakagawa and K. Tomishige, *J. Catal.*, 2011, **280**, 221-229.
[25] S. Koso, H. Watanabe, K. Okumura, Y. Nakagawa and K. Tomishige, *Appl. Catal. B: Environ.*, 2012, **111-112**, 27-37.
[26] S. Koso, H. Watanabe, K. Okumura, Y. Nakagawa and K. Tomishige, *J. Phys. Chem. C*, 2012, **116**, 3079-3090.
[27] K. Y. Chen, K. Mori, H. Watanabe, Y. Nakagawa and K. Tomishige, *J. Catal.*, 2012, **294**, 171-183.

[28] M. Chia, Y.J.P. Torres, D. Hibbitts, Q. Tan, H.N. Pham, A.K. Datye, M. Neurock, R.J. Davis and J.A. Dumesic, *J. Am. Chem. Soc.*, 2011, **133**, 12675-12689.
[29] M. Chatterjee, H. Kawanami, T. Ishizaka, M. Sato, T. Suzuki and A. Suzuki, *Catal. Sci.Technol.*, 2011, **1**, 1466-1471.
[30] H. Adkins and R. Connor, *J. Am. Chem. Soc.*, 1931, **53**, 1091–1095.
[31] R. Connor and H. Adkins, *J. Am. Chem. Soc.*, 1932, **54**, 4678–4690.
[32] W. Xu, H. Wang, X. Liu, J. Ren, Y. Wang and G. Lu, *Chem. Commun.*, 2011, **47**, 3924–3926.
[33] S. B. Liu, Y. Amada, M. Tamura, Y. Nakagawa and K. Tomishige, *Green Chem.*, 2014, **16**, 617-626.
[34] K. Zeitsch, *The Chemistry and Technology of Furfural and its Many By-Products*, Elsevier Science, Amsterdam, 2000
[35] K. Y. Chen, M. Tamura, Z. L. Yuan, Y. Nakagawa and K. Tomishige, *ChemSusChem*, 2013, **6**, 613-621.
[36] J.W. Cook and D.E. Sayers, *J. Appl. Phys.*, 1981, **52**, 5024-5031.
[37] K. Okumura, J. Amano, N. Yasunobu and M. Niwa, *J. Phys. Chem. B*, 2000, **104**, 1050-1057.
[38] K. Okumura, S. Matsumoto, N. Nishiaki and M. Niwa, *Appl. Catal. B: Environ.*, 2003, **40**, 151-159.
[39] A.L. Ankudinov, B. Ravel, J.J. Rehr and S.D. Conradson, *Phys. Rev. B*, 1998, **58**, 7565-7576.
[40] K. Tomishige, K. Asakura and Y. Iwasawa, *J. Catal.*, 1994, **149**, 70-80.
[41] R. Alamillo, M. Tucker, M. Chia, Y. Pagán-Torres and J. Dumesic, *Green Chem.*, 2012, **14**, 1413-1419.
[42] S. Sitthisa and D. E. Resasco, *Catal. Lett.*, 2011, **141**, 784-791.
[43] D. E. Resasco, S. Sitthisa, J. F. T. Prasomsri and M. Pilar ruiz, *Heterogeneous in biomass to Chemicals and Fuels*, Research Signpost, 2012, 155-188.
[44] Y. Amada, Y. Shinmi, S. Koso, T. Kubota, Y. Nakagawa and K. Tomishige, *Appl. Catal. B: Environ.*, 2011, 105, 117-127.
[45] Y. Nakagawa, X. H. Ning, Y. Amada and K. Tomishige, *Appl. Catal. A: Gen.*, 2012, **433-434**, 128-134
[46] Y. Amada, H. Watanabe, M. Tamura, Y. Nakagawa, K. Okumura and K. Tomishige, *J. Phys. Chem. C* 2012,**116**, 23503-23514.
[47] Y. Shinmi, S. Koso, T. Kubota, Y. Nakagawa and K. Tomishige, *Appl. Catal. B: Environ.*, 2010, **94**, 318-326.
[48] T. Ebashi, Y. Ishida, Y. Nakagawa, S.-i. Ito, T. Kubota and K. Tomishige, *J. Phys. Chem. C*, 2010, **114**, 6518-6526.
[49] Y. Ishida, T. Ebashi, S.-i. Ito, T. Kubota, K. Kunimori and K. Tomishige, *Chem. Commun.*, 2009, 5308-5310.
[50] X. Hong, B. Li, Y. J. Wang, J. Q. Lu, G. S. Hu and M. F. Luo, *Appl. Surf. Sci.*, 2013, **270**, 388-394.
[51] H.-D. Kim, H. J. Park, T.-W. Kim, K.-E. Jeong, H.-J. Chae, S.-Y. Jeong, C.-H. Lee and C.-U. Kim, *Catal. Today*, 2012, **185**, 73-80.
[52] http://www.asminternational.org/asmenterprise/apd.
[53] M. Tamura, Y. Amada, S. B. Liu, Z. L. Yuan, Y. Nakagawa and K. Tomishige, *J. Mol. Catal. A: Chem.*, 2013, DOI: 10.1016/j.molcata.2013.09.015.
[54] A.C. Yang and C. W. Garland, *J. Phys. Chem.*, 1957, **61**, 1504-1512.

[55] P. Basu, D. Panayotov and J. T. Yates, *J. Phy. Chem.*, 1987, **91**, 3133-3136.
[56] P. Basu, D. Panayotov and J. T. Yates, *J. Am. Chem. Soc.*, 1988, **110**, 2074-2081.

Table 1. Conversion of furfural over different catalysts at low temperature step

Entry	Catalysts	T_1 / K	Time 1 / h	T_2 / K	Time 2 / h	Conversion / %	Yield / %									
							1,5-PeD	1,4-PeD	1,2-PeD	1-PeOH	2-PeOH	THFA	FFA	2-MTHF	1,2,5-PeT	Others
1	Ir-ReO_x/SiO_2	313	8	-	-	>99.9	0.0	0.0	0.3	0.2	0.0	0.5	96.9	0.6	0.0	< 2.0
2	Rh(0.66)-Ir-ReO_x/SiO_2	313	8	-	-	>99.9	0.4	0.2	0.4	0.2	0.0	58.2	14.4	1.4	4.8	19.8
3	Pd(0.66)-Ir-ReO_x/SiO_2	313	8	-	-	>99.9	0.0	1.6	0.3	0.1	0.0	66.8	0.0	3.6	6.5	21.0
4	Rh(0.66)/SiO_2+Ir-ReO_x/SiO_2[a]	313	8	-	-	>99.9	0.2	0.1	0.5	0.2	0.0	6.6	86.6	0.7	0.0	5.3
5	Rh(0.66)-Ir/SiO_2+Ir-ReO_x/SiO_2[b]	313	8	-	-	>99.9	0.3	0.7	0.5	0.4	0.0	21.5	55.7	1.2	0.0	19.8
6	Rh(0.66)-ReO_x /SiO_2+Ir-ReO_x/SiO_2[c]	313	8	-	-	>99.9	0.0	0.0	0.0	0.0	0.0	1.9	81.7	0.9	0.0	15.6
7	Pd(0.66)/SiO_2+Ir-ReO_x/SiO_2[d]	313	8	-	-	>99.9	0.1	0.5	0.3	0.1	0.0	49.3	8.8	2.8	1.4	36.7
8	Ir-ReO_x/SiO_2	313	8	373	0	>99.9	0.0	0.1	0.6	0.3	0.0	0.9	87.9	1.9	0.0	8.3
9	Rh(0.66)-Ir-ReO_x/SiO_2	313	8	373	0	>99.9	0.6	0.7	0.5	0.2	0.0	67.3	0.3	1.5	11.1	17.7
10	Pd(0.66)-Ir-ReO_x/SiO_2	313	8	373	0	>99.9	0.2	3.1	0.3	0.1	0.0	69.7	0.0	3.2	11.5	11.8
11	Rh(0.66)/SiO_2+Ir-ReO_x/SiO_2[a]	313	8	373	0	>99.9	0.2	0.1	0.7	0.2	0.0	11.0	61.3	1.4	0.0	25.1
12	Rh(0.66)-Ir/SiO_2+Ir-ReO_x/SiO_2[b]	313	8	373	0	>99.9	0.4	0.8	0.7	0.5	0.0	31.2	22.2	1.6	1.4	41.2
13	Rh(0.66)-ReO_x /SiO_2+Ir-ReO_x/SiO_2[c]	313	8	373	0	>99.9	0.1	0.6	0.5	0.4	0.0	4.8	59.9	2.7	0.0	30.9
14	Pd(0.66)/SiO_2+Ir-ReO_x/SiO_2[d]	313	8	373	0	>99.9	0.3	2.9	0.4	0.1	0.1	56.4	0.1	3.4	6.8	29.7

PeD: pentanediol; PeOH: pentanol; THFA: tetrahydrofurfuryl alcohol; FFA: furfuryl alcohol; 2-MTHF: 2-methyltetrahydrofuran; PeT: pentanetriol; Others: unidentified products.

Pretreatment: 473 K, H_2 (8 MPa), 1 h.

Reaction conditions: furfural (3 g), H_2O (3 g), catalyst (Re/Ir=2; 300 mg), initial H_2 (6 MPa).

a: Physical mixture of Rh(0.66)/SiO_2 and Ir-ReO_x/SiO_2 with the same metal amount as Rh(0.66)-Ir-ReO_x/SiO_2. b: Physical mixture of Rh(0.66)-Ir/SiO_2 (300 mg) and Ir-ReO_x/SiO_2 (300 mg). c: Physical mixture of Rh(0.66)-ReO_x/SiO_2 (300 mg) and Ir-ReO_x/SiO_2 (300 mg). d: Physical mixture of Pd(0.66)/SiO_2 and Ir-ReO_x/SiO_2 with the same metal amount as Pd(0.66)-Ir-ReO_x/SiO_2.

Table 2. Conversion of furfural over different catalysts from low temperature step to high temperature step

Entry	Catalysts	T_1 / K	Time 1 / h	T_2 / K	Time 2 / h	Conversion / %	Yield / %									
							1,5-PeD	1,4-PeD	1,2-PeD	1-PeOH	2-PeOH	THFA	FFA	2-MTHF	1,2,5-PeT	Others
1	Ir-ReO_x/SiO_2	313	8	373	24	>99.9	1.4	1.1	0.3	0.4	0.0	0.4	9.7	1.2	0.0	85.4
2	Rh(0.1)-Ir-ReO_x/SiO_2	313	8	373	24	>99.9	2.6	12.2	1.1	0.7	0.3	20.3	0.4	3.5	14.4	44.5
3	Rh(0.3)-Ir-ReO_x/SiO_2	313	8	373	24	>99.9	58.6	5.2	1.2	7.3	0.5	8.3	0.0	2.2	9.4	7.3
4	Rh(0.5)-Ir-ReO_x/SiO_2	313	8	373	24	>99.9	64.4	4.1	0.9	7.2	0.3	7.8	0.0	2.3	6.5	6.3
5	Rh(0.66)-Ir-ReO_x/SiO_2	313	8	373	24	>99.9	65.8	3.9	0.6	7.5	0.3	7.1	0.0	2.4	3.6	9.0
6	Rh(0.75)-Ir-ReO_x/SiO_2	313	8	373	24	>99.9	62.7	3.6	0.7	8.0	0.3	9.3	0.0	2.0	2.8	10.7
7	Rh(1)-Ir-ReO_x/SiO_2	313	8	373	24	>99.9	59.3	3.4	0.7	5.4	0.2	14.7	0.0	2.1	3.7	10.6
8	Rh(2)-Ir-ReO_x/SiO_2	313	8	373	24	>99.9	53.6	3.5	0.6	6.8	0.3	10.3	0.0	2.7	2.8	19.3
9	Pd(0.66)-Ir-ReO_x/SiO_2	313	8	373	24	>99.9	44.5	6.1	0.5	3.3	0.3	20.9	0.0	3.7	4.6	16.0
10	Pd(0.66)-Ir-ReO_x/SiO_2	313	8	373	48	>99.9	61.5	5.4	0.4	13.2	0.7	5.0	0.0	5.0	3.3	5.4
11	Rh(0.66)/SiO_2+Ir-ReO_x/SiO_2[a]	313	8	373	24	>99.9	2.1	12.7	0.6	0.4	0.1	14.5	0.3	2.4	5.7	61.1
12	Pd(0.66)/SiO_2+Ir-ReO_x/SiO_2[b]	313	8	373	24	>99.9	35.0	4.7	0.3	2.2	0.2	16.4	0.0	3.8	4.0	33.5
13	Rh(0.66)-Ir/SiO_2+Ir-ReO_x/SiO_2[c]	313	8	373	24	>99.9	8.0	12.9	1.1	0.9	0.3	31.4	0.0	4.8	11.0	29.7
14	Rh(0.66)- ReO_x /SiO_2+Ir-ReO_x/SiO_2[d]	313	8	373	24	>99.9	0.1	9.4	0.6	0.4	0.0	7.4	3.6	2.5	0.0	75.9
15[e]	Rh(0.66)-Ir-ReO_x/SiO_2	313	8	373	24	>99.9	72.4	2.8	0.7	6.3	0.2	11.8	0.0	1.4	3.5	< 2.0
16[e]	Rh(0.66)-Ir-ReO_x/SiO_2	313	8	373	32	>99.9	78.2	2.8	1.2	9.5	0.2	6.4	0.0	1.4	2.0	< 2.0
17[e]	Pd(0.66)-Ir-ReO_x/SiO_2	313	8	373	24	>99.9	55.6	5.8	0.8	3.5	0.2	24.6	0.0	2.5	3.8	3.4

PeD: pentanediol; PeOH: pentanol; THFA: tetrahydrofurfuryl alcohol; FFA: furfuryl alcohol; 2-MTHF: 2-methyltetrahydrofuran; PeT: pentanetriol; Others: unidentified products.

Pretreatment: 473 K, H_2 (8 MPa), 1 h.

Reaction conditions: furfural (3 g), H_2O (3 g), catalyst (Re/Ir=2; 300 mg), initial H_2 (6 MPa). e: furfural (1g), H_2O (9 g), catalyst (Re/Ir=2; 100 mg), initial H_2 (6 MPa).

a: Physical mixture of Rh(0.66)/SiO_2 and Ir-ReO_x/SiO_2 with the same metal amount as Rh(0.66)-Ir-ReO_x/SiO_2. b: Physical mixture of Rh(0.66)-Ir/SiO_2 (300 mg) and Ir-ReO_x/SiO_2 (300 mg). c: Physical mixture of Rh(0.66)-ReO_x/SiO_2 (300 mg) and Ir-ReO_x/SiO_2 (300 mg). d: Physical mixture of Pd(0.66)/SiO_2 and Ir-ReO_x/SiO_2 with the same metal amount as Pd(0.66)-Ir-ReO_x/SiO_2.

Table 3. Hydrogenolysis of THFA over different catalysts

Catalysts	Conversion	Selectivity / %				
(Re/Ir=2)	/ %	1,5-PeD	1,2-PeD	1-PeOH	2-PeOH	Others
Ir-ReO_x/SiO_2	63.7	92.8	0.0	6.9	0.0	0.3
Pd(0.66)-Ir-ReO_x/SiO_2	39.0	94.7	0.0	4.8	0.0	0.5
Rh(0.66)-Ir-ReO_x/SiO_2	53.6	95.2	0.0	4.2	0.0	0.5

PeD: pentanediol; PeOH: pentanol; Others: 2-methyltetrahydrofuran+1-butanol+pentane.

Pretreatment: 473 K, H_2 (8 MPa), 1 h.

Reaction conditions: THFA (3 g), H_2O (3 g), catalyst (300 mg), H_2 (6 MPa), 373 K, 2 h.

Table 4. Conversion of furfural over Rh(0.66)-Ir-ReO_x/SiO_2 at different temperature.

Entry	T_1 / K	Time 1 / h	T_2 / K	Time 2 / h	Conversion / %	Yield / %									
						1,5-PeD	1,4-PeD	1,2-PeD	1-PeOH	2-PeOH	THFA	FFA	2-MTHF	1,2,5-PeT	Others
1	303	8	-	-	>99.9	0.2	0.5	0.0	0.3	0.0	52.5	25.3	0.5	3.7	16.9
2	313	8	-	-	>99.9	0.4	0.2	0.4	0.2	0.0	58.2	14.4	1.4	4.8	19.8
3	323	8	-	-	>99.9	0.2	0.6	0.0	0.3	0.0	62.0	13.1	0.8	4.0	19.0
4	333	8	-	-	>99.9	0.5	1.0	0.0	0.4	0.0	57.6	4.2	1.7	4.2	30.3
5	303	8	373	24	>99.9	66.4	3.8	0.5	7.6	0.3	7.8	0.0	2.4	4.5	6.6
6	313	8	373	24	>99.9	65.8	3.9	0.6	7.5	0.3	8.3	0.0	2.4	3.2	8.1
7	323	8	373	24	>99.9	60.8	4.7	0.7	6.8	0.4	7.5	0.0	2.4	6.4	10.4
8	333	8	373	24	>99.9	53.8	5.2	0.7	5.7	0.3	11.7	0.0	2.6	7.3	12.7
9	313	8	353	24	>99.9	38.5	3.9	0.6	1.4	0.1	31.7	0.0	2.1	15.6	6.1
10	313	8	373	24	>99.9	65.8	3.9	0.6	7.5	0.3	8.3	0.0	2.4	3.2	8.1
11	313	8	393	24	>99.9	57.3	5.5	0.6	17.3	1.1	1.7	0.0	4.5	1.3	10.7
12	313	8	413	24	>99.9	37.7	3.1	0.2	34.6	1.9	1.0	0.0	5.5	0.0	15.9

PeD: pentanediol; PeOH: pentanol; THFA: tetrahydrofurfuryl alcohol; FFA: furfuryl alcohol; 2-MTHF: 2-methyltetrahydrofuran; PeT: pentanetriol; Others: unidentified products.

Pretreatment: 473 K, H_2 (8 MPa), 1 h.

Reaction conditions: furfural (3 g), H_2O (3 g), catalyst (Re/Ir=2; 300 mg), initial H_2 (6 MPa).

Table 5. Conversion of furfural over Rh(0.66)-Ir-ReO_x/SiO_2 at different pressure.

Entry	Pressure / MPa	Conversion / %	Yield / %									
			1,5-PeD	1,4-PeD	1,2-PeD	1-PeOH	2-PeOH	THFA	FFA	2-MTHF	1,2,5-PeT	Others
1	2	>99.9	1.5	0.7	0.1	0.2	0.0	6.0	0.1	0.3	0.0	91.2
2	4	>99.9	6.9	12.1	0.4	0.6	0.2	30.1	0.0	3.1	14.8	31.7
3	6	>99.9	65.8	3.9	0.6	7.5	0.3	8.3	0.0	2.4	3.2	8.1
4	8	>99.9	71.1	3.4	0.5	10.8	0.3	4.8	0.0	2.2	1.8	5.2
5	10	>99.9	69.8	3.8	0.5	14.0	0.4	5.6	0.0	2.5	1.8	< 2.0

PeD: pentanediol; PeOH: pentanol; THFA: tetrahydrofurfuryl alcohol; FFA: furfuryl alcohol; 2-MTHF: 2-methyltetrahydrofuran; PeT: pentanetriol; Others: unidentified products.

Pretreatment: 473 K, H_2 (8 MPa), 1 h.

Reaction conditions: furfural (3 g), H_2O (3 g), catalyst (Re/Ir=2; 300 mg), T_1: 313 K, Time 1: 8 h, T_2: 373 K, Time 2: 24 h.

Table 6. Reuse of Rh(0.66)-Ir-ReO_x/SiO_2 for conversion of furfural.

Usage times	Calcined temperature / K	Conversion / %	Yield / %										Re leaching amount / %
			1,5-PeD	1,4-PeD	1,2-PeD	1-PeOH	2-PeOH	THFA	FFA	2-MTHF	1,2,5-PeT	Others	
1	-	>99.9	65.8	3.9	0.6	7.5	0.3	8.3	0.0	2.4	3.2	8.1	2.8
2	773	>99.9	54.6	3.4	0.7	4.0	0.2	22.0	0.0	1.6	7.6	5.9	0.8
3	773	>99.9	47.9	3.4	0.7	2.6	0.2	24.3	0.2	1.6	8.8	10.3	2.1
2	573	>99.9	54.6	4.5	1.1	5.1	0.3	14.9	0.0	2.1	9.4	8.0	0.8
3	573	>99.9	16.9	4.7	1.3	1.1	0.2	44.1	0.2	1.6	19.6	10.4	5.0
1[a]	-	>99.9	72.4	2.8	0.7	6.3	0.2	11.8	0.0	1.4	3.5	< 2.0	0.4
2[a]	773	>99.9	61.2	2.6	0.6	3.1	0.1	26.3	0.0	1.1	4.1	< 2.0	0.2
3[a]	773	>99.9	45.3	2.7	0.5	1.6	0.1	32.0	0.0	1.2	7.8	8.7	0.2

PeD: pentanediol; PeOH: pentanol; THFA: tetrahydrofurfuryl alcohol; FFA: furfuryl alcohol; 2-MTHF: 2-methyltetrahydrofuran; PeT: pentanetriol.

Pretreatment: 473 K, H_2 (8 MPa), 1 h. Calcination time before reuse: 3 h.

Reaction conditions: furfural (3 g), H_2O (3 g), catalyst (Re/Ir=2; 300 mg), a: furfural (1 g), H_2O (9 g), catalyst (Re/Ir=2; 100 mg). T_1: 313 K, Time 1: 8 h, T_2: 373 K, Time 2: 24 h.

Table 7. Summary of characterization results

Catalyst	Metal amount / mmol·g_{cat}^{-1}			TPR		Re L_3-edge XANES	CO adsorption	Dispersion[b]
	Rh	Ir	Re	H_2 consumption / mmol·g_{cat}^{-1}	Valence of Re[a]	Valence of Re	/ mmol·g_{cat}^{-1}	/ %
Ir-ReO_x/SiO_2	–	0.208	0.416	0.927	4.5	3.1	0.037	18
Rh-ReO_x/SiO_2	0.064	–	0.416	1.05	2.4		0.037	52
Rh(0.1)-Ir-ReO_x/SiO_2	0.010	0.208	0.416	1.27	3.0		0.061	28
Rh(0.3)-Ir-ReO_x/SiO_2	0.029	0.208	0.416	1.41	2.4		0.062	26
Rh(0.5)-Ir-ReO_x/SiO_2	0.049	0.208	0.416	1.36	2.8		0.060	23
Rh(0.66)-Ir-ReO_x/SiO_2	0.064	0.208	0.416	1.35	3.0	2.4	0.066	24
Rh(0.75)-Ir-ReO_x/SiO_2	0.073	0.208	0.416	1.28	3.4		0.068	24
Rh(1)-Ir-ReO_x/SiO_2	0.097	0.208	0.416	1.36	3.2	2.3	0.070	23
Rh(2)-Ir-ReO_x/SiO_2	0.194	0.208	0.416	1.40	3.7	2.4	0.092	23
Rh(0.66)/SiO_2	0.064	–	–	–	–		0.032	49
Rh(0.66)-Ir/SiO_2	0.064	0.208	–	–	–		0.036	13

a: 7-2×[(amount of H_2 consumed, mol)-2×(Ir loading amount, mol)-3/2×(Rh loading amount, mol)]/(Re loading amount, mol).

b: Dispersion (%) = [CO adsorption amount]/[(Ir loading amount) +(Rh loading amount)] ×100

Table 8 Curve fitting results of Ir L_3-edge EXAFS of Ir-ReO_x/SiO_2 and Rh-Ir-ReO_x/SiO_2 after the reduction.

Catalyst	Shells	CN[a]	R / 10^{-1} nm[b]	σ / 10^{-1} nm[c]	ΔE_0 / eV[d]	R_f / %[e]
Ir-ReO_x/SiO_2[f]	Ir-Ir (or -Re)	10.6 ± 0.9	2.76 ± 0.01	0.067 ± 0.004	−1.0 ± 1.2	0.9
Rh(0.66)-Ir-ReO_x/SiO_2	Ir-Ir (or -Re)	8.6 ± 0.9	2.76 ± 0.01	0.068 ± 0.004	−1.2 ± 1.1	1.6
	Ir-Rh	2.2 ± 0.4	2.72 ± 0.02	0.081 ± 0.006	9.8 ± 3.5	
Rh(1)-Ir-ReO_x/SiO_2	Ir-Ir (or -Re)	8.5 ± 0.8	2.77 ± 0.01	0.069 ± 0.003	−0.2 ± 1.2	1.7
	Ir-Rh	2.4 ± 0.3	2.72 ± 0.02	0.081 ± 0.005	9.2 ± 3.5	
Rh(2)-Ir-ReO_x/SiO_2	Ir-Ir (or -Re)	7.9 ± 0.7	2.77 ± 0.01	0.069 ± 0.004	0.6 ± 1.3	2.2
	Ir-Rh	2.8 ± 0.5	2.71 ± 0.01	0.079 ± 0.005	9.9 ± 2.7	
Ir powder	Ir-Ir	12	2.77	0.06	0	–

[a]Coordination number. [b]Bond distance. [c]Debye-Waller factor. [d]Difference in the origin of photoelectron energy between the reference and the sample.

[e]Residual factor. [f]After glycerol hydrogenolysis[44]. Fourier filtering range: 0.163-0.325 nm.

Table 9 Curve fitting results of Re L_3-edge EXAFS of Ir-ReO_x/SiO_2 and Rh-Ir-ReO_x/SiO_2 after the reduction.

Catalyst	Shells	CN[a]	R / 10^{-1} nm[b]	σ / 10^{-1} nm[c]	ΔE_0 / eV[d]	R_f / %[e]
Ir-ReO_x/SiO_2[f]	Re-O	1.7 ± 0.5	2.03 ± 0.03	0.080 ± 0.016	0.6 ± 5.0	2.5
	Re-Ir (or -Re)	6.1 ± 1.1	2.68 ± 0.01	0.082 ± 0.006	8.1 ± 1.8	
Rh(0.66)-Ir-ReO_x/SiO_2	Re-O	1.4 ± 0.4	2.04 ± 0.02	0.085 ± 0.010	−2.1 ± 3.6	1.9
	Re-Ir (or -Re)	5.9 ± 0.4	2.67 ± 0.01	0.087 ± 0.002	6.6 ± 1.2	
Rh(1)-Ir-ReO_x/SiO_2	Re-O	1.0 ± 0.2	2.04 ± 0.03	0.085 ± 0.008	−3.0 ± 6.0	2.2
	Re-Ir (or -Re)	5.7 ± 0.6	2.67 ± 0.01	0.086 ± 0.004	5.8 ± 1.2	
	Re-Rh	0.4 ± 0.2	2.64 ± 0.02	0.062 ± 0.014	−1.3 ± 6.2	
Rh(2)-Ir-ReO_x/SiO_2	Re-O	1.3 ± 0.4	2.05 ± 0.03	0.086 ± 0.009	−1.3 ± 4.1	2.3
	Re-Ir (or -Re)	5.3 ± 0.6	2.66 ± 0.01	0.087 ± 0.003	5.1 ± 1.4	
	Re-Rh	0.7 ± 0.1	2.63 ± 0.01	0.061 ± 0.005	−6.0 ± 2.9	
NH_4ReO_4	Re=O	4	1.73	0.06	0	–

[a]Coordination number. [b]Bond distance. [c]Debye-Waller factor. [d]Difference in the origin of photoelectron energy between the reference and the sample. [e]Residual factor. [f]After glycerol hydrogenolysis[44]. Fourier filtering range: 0.138-0.325 nm.

Table 10 Curve fitting results of Rh *K*-edge EXAFS of Rh-Ir-ReO_x/SiO_2 after the reduction.

Catalyst	Shells	CN[a]	R / 10^{-1} nm[b]	σ / 10^{-1} nm[c]	ΔE_0 / eV[d]	R_f / %[e]
Rh(0.66)-Ir-ReO_x/SiO_2	Rh-Rh	2.0 ± 0.5	2.68 ± 0.02	0.087 ± 0.007	–1.7 ± 3.9	2.2
	Rh-Ir (or -Re)	7.0 ± 0.6	2.69 ± 0.01	0.078 ± 0.003	–1.8 ± 1.1	
Rh(1)-Ir-ReO_x/SiO_2	Rh-Rh	2.8 ± 0.6	2.68 ± 0.01	0.085 ± 0.008	–4.5 ± 2.6	2.3
	Rh-Ir (or -Re)	6.2 ± 0.6	2.69 ± 0.01	0.082 ± 0.003	0.1 ± 1.1	
Rh(2)-Ir-ReO_x/SiO_2	Rh-Rh	4.9 ± 0.5	2.68 ± 0.01	0.082 ± 0.004	0.0 ± 1.2	2.1
	Rh-Ir (or -Re)	4.2 ± 0.9	2.69 ± 0.01	0.086 ± 0.004	2.5 ± 2.2	
Rh foil	Rh-Rh	12	2.68	0.06	0	–

[a]Coordination number. [b]Bond distance. [c]Debye-Waller factor. [d]Difference in the origin of photoelectron energy between the reference and the sample. [e]Residual factor. Fourier filtering range: 0.163-0.310 nm.

Figure captions

Fig. 1. Time course of conversion of furfural to 1,5-PeD over Rh(0.66)-Ir-ReO_x/SiO_2 or Pd(0.66)-Ir-ReO_x/SiO_2

Scheme 1 Possible reaction routes of conversion of furfural.

Fig. 2. TPR profiles of the catalysts. (a) Rh/SiO_2 (Rh=0.66 wt%), (b) Ir/SiO_2 (Ir=4 wt%), (c) ReO_x/SiO_2 (Re=7.8 wt%), (d) Rh-Ir/SiO_2 (Rh=0.66 wt%, Ir=4 wt%), (e) Rh-ReO_x/SiO_2 (Rh=0.66 wt%, Re=7.8 wt%), (f) Ir-ReO_x/SiO_2 (Ir=4 wt%, Re/Ir=2), (g) Rh(0.1)-Ir-ReO_x/SiO_2, (h) Rh(0.3)-Ir-ReO_x/SiO_2, (i) Rh(0.5)-Ir-ReO_x/SiO_2, (j) Rh(0.66)-Ir-ReO_x/SiO_2, (k) Rh(0.75)-Ir-ReO_x/SiO_2, (l) Rh(1)-Ir-ReO_x/SiO_2 and (m) Rh(2)-Ir-ReO_x/SiO_2.

Fig. 3. Results of Re L_3-edge XANES analysis of Ir-ReO_x/SiO_2 and Rh-Ir-ReO_x/SiO_2 after the reduction. (I) Re L_3-edge XANES spectra, (II) Relation between white line area and valence of Re. (a) Re powder, (b) Ir-ReO_x/SiO_2 after glycerol hydrogenolysis[44], (c) Rh(0.66)-Ir-ReO_x/SiO_2, (d) Rh(1)-Ir-ReO_x/SiO_2, (e) Rh(2)-Ir-ReO_x/SiO_2 after the reduction, (f) ReO_2, (g) ReO_3 and (h) Re_2O_7.

Fig. 4. XRD patterns of catalysts. (a) Ir/SiO_2 (Ir=4 wt%), (b) Rh/SiO_2 (Rh=0.66 wt%), (c) ReO_x/SiO_2 (Re=7.8 wt%), (d) Rh-ReO_x/SiO_2 (Rh=0.66 wt%, Re=7.8 wt%), (e) Rh-Ir/SiO_2 (Rh=0.66 wt%, Ir=4 wt%), (f) Ir-ReO_x/SiO_2 (Ir=4 wt%, Re/Ir=2) after reduction at 473 K for 1 h. (g) Rh(0.1)-Ir-ReO_x/SiO_2, (h) Rh(0.3)-Ir-ReO_x/SiO_2, (i) Rh(0.5)-Ir-ReO_x/SiO_2, (j) Rh(0.66)-Ir-ReO_x/SiO_2, (k) Rh(0.75)-Ir-ReO_x/SiO_2, (l) Rh(1)-Ir-ReO_x/SiO_2 and (m) Rh(2)-Ir-ReO_x/SiO_2 after reaction. (A) 2 theta range 30-75°, (B) 2 theta range 38-46°.

Fig. 5. Results of Ir L_3-edge EXAFS analysis of Ir-ReO_x/SiO_2 and Rh-Ir-ReO_x/SiO_2 after the reduction. (I) k^3-Weighted EXAFS oscillations. (II) Fourier transform of k^3-weighted Ir L_3-edge EXAFS, FT range: 30–130nm^{-1}. (III) Fourier filtered EXAFS data (solid line) and calculated data (dotted line), Fourier filtering range: 0.163-0.325 nm. (a) Ir powder, (b) IrO_2, (c) Ir-ReO_x/SiO_2 after glycerol hydrogenolysis[44] and (d-f) Rh−Ir−ReO_x/SiO_2 after the reduction ((d) Rh = 0.66 wt%, (e) Rh =1 wt% and (f) Rh = 2 wt%).

Fig. 6. Results of Re L_3-edge EXAFS analysis of Ir-ReO_x/SiO_2 and Rh-Ir-ReO_x/SiO_2 after the reduction. (I) k^3-Weighted EXAFS oscillations. (II) Fourier transform of k^3-weighted Re L_3-edge EXAFS, FT range: 30–120 nm^{-1}. (III) Fourier filtered EXAFS data (solid line) and calculated data (dotted line), Fourier filtering range: 0.138–0.325 nm. (a) Re powder, (b) NH_4ReO_4, (c) Ir-ReO_x/SiO_2 after glycerol hydrogenolysis[44] and (d-f) Rh-Ir-ReO_x/SiO_2 after the reduction ((d) Rh = 0.66 wt%, (e) Rh =1 wt% and (f) Rh = 2 wt%).

Fig. 7. Results of Rh K-edge EXAFS analysis of Rh−Ir−ReO_x/SiO_2 after the reduction.

(I) k^3-Weighted EXAFS oscillations. (II) Fourier transform of k^3-weighted Rh *K*-edge EXAFS, FT range: 30–130 nm^{-1}. (III) Fourier filtered EXAFS data (solid line) and calculated data (dotted line), Fourier filtering range: 0.163–0.310 nm. (a) Rh foil, (b) Rh_2O_3, (c-e) Rh−Ir−ReO_x/SiO_2 after the reduction ((c) Rh = 0.66 wt%, (d) Rh =1 wt% and (e) Rh = 2 wt%) .

Fig. 8. TEM image and STEM-EDX mappings of Rh(0.66)-Ir-ReO_x/SiO_2 after reduction. The maps reflect the measured (b) Si K intensity, (c) O K intensity, (d) Ir M intensity, (e) Rh L intensity, (f) Re M intensity.

Fig. 9. DRIFT spectra of CO adsorbed on the catalysts after reduction at 473 K. (a) Rh/SiO_2 (Rh=0.66 wt%), (b) Ir-ReO_x/SiO_2 (Ir=4 wt%, Re/Ir=2), (c) Rh(0.66)-Ir-ReO_x/SiO_2, (d) Rh(1)-Ir-ReO_x/SiO_2 and (e) Rh(2)-Ir-ReO_x/SiO_2.

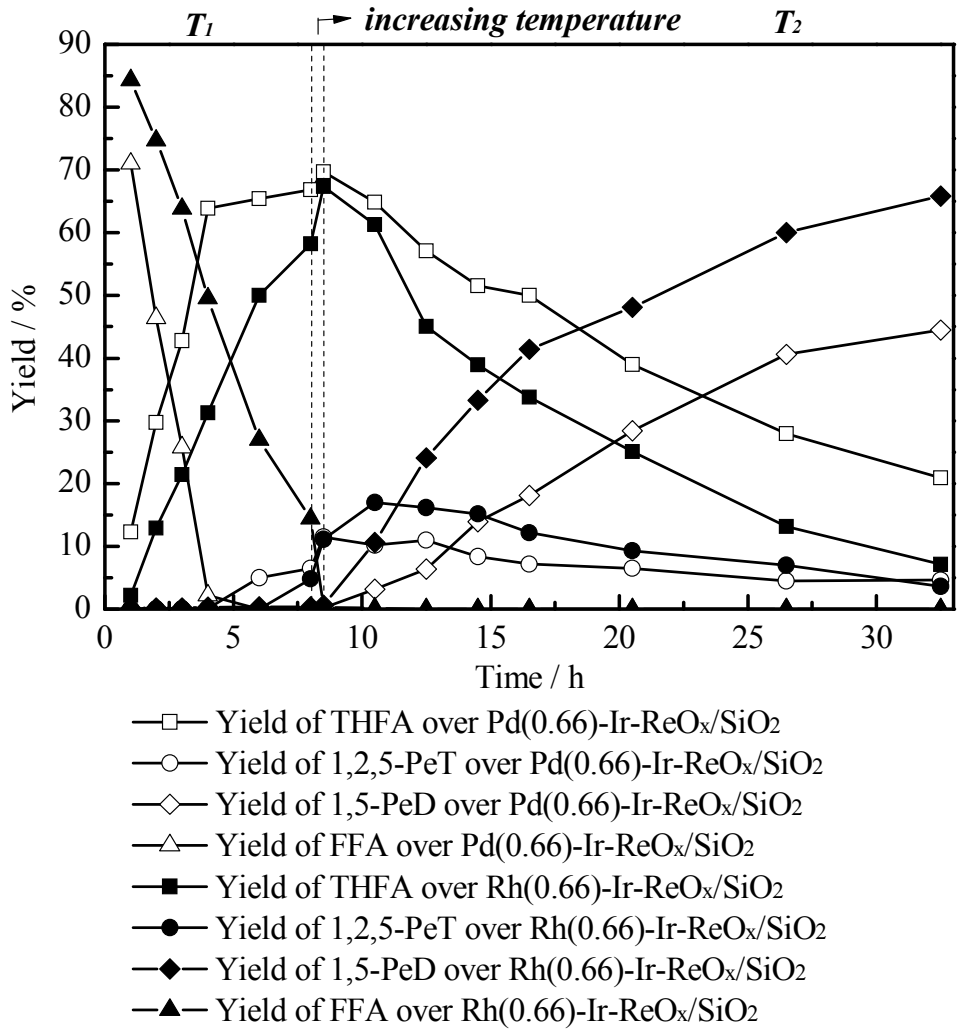

Fig. 1. Time course of conversion of furfural to 1,5-PeD over Rh(0.66)-Ir-ReO_x/SiO_2 or Pd(0.66)-Ir-ReO_x/SiO_2 Conditions: furfural (3 g), H_2O (3 g), catalyst (300 mg), initial H_2 (6 MPa), T_1: 313 K, T_2: 373 K.

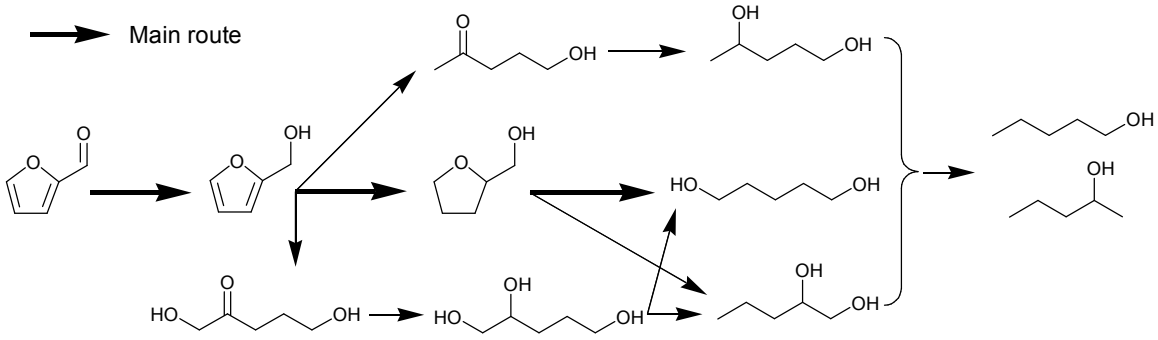

Scheme 1 Possible reaction routes of conversion of furfural.

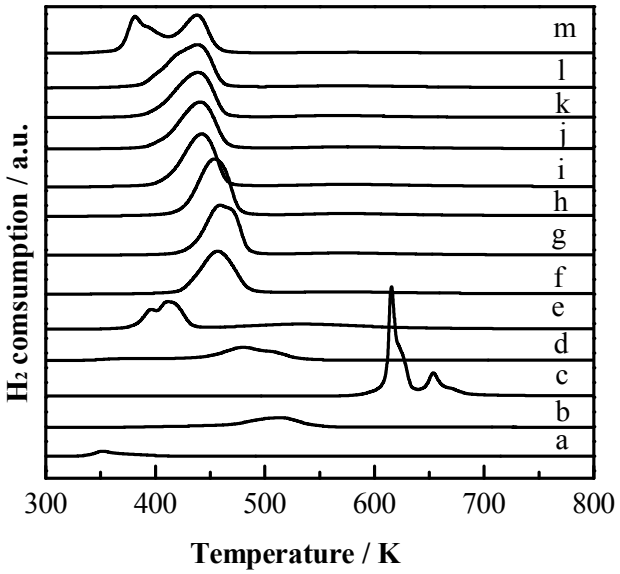

Fig. 2. TPR profiles of the catalysts. (a) Rh/SiO_2 (Rh=0.66 wt%), (b) Ir/SiO_2 (Ir=4 wt%), (c) ReO_x/SiO_2 (Re=7.8 wt%), (d) $Rh\text{-}Ir/SiO_2$ (Rh=0.66 wt%, Ir=4 wt%), (e) $Rh\text{-}ReO_x/SiO_2$ (Rh=0.66 wt%, Re=7.8 wt%), (f) $Ir\text{-}ReO_x/SiO_2$ (Ir=4 wt%, Re/Ir=2), (g) $Rh(0.1)\text{-}Ir\text{-}ReO_x/SiO_2$, (h) $Rh(0.3)\text{-}Ir\text{-}ReO_x/SiO_2$, (i) $Rh(0.5)\text{-}Ir\text{-}ReO_x/SiO_2$, (j) $Rh(0.66)\text{-}Ir\text{-}ReO_x/SiO_2$, (k) $Rh(0.75)\text{-}Ir\text{-}ReO_x/SiO_2$, (l) $Rh(1)\text{-}Ir\text{-}ReO_x/SiO_2$ and (m) $Rh(2)\text{-}Ir\text{-}ReO_x/SiO_2$. Y-axis is normalized by the weight of the sample. Conditions: sample (50 mg, calcined at 773 K for 3 h) and H_2/Ar (5% v/v, 30 ml min^{-1}) at the heating rate of 10 K min^{-1}.

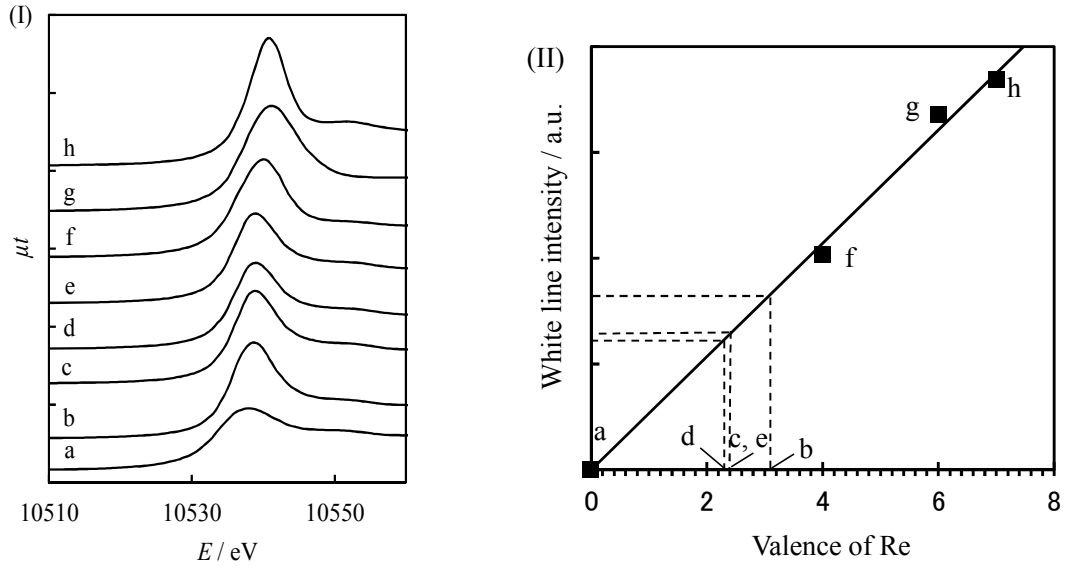

Fig. 3. Results of Re L_3-edge XANES analysis of Ir-ReO_x/SiO_2 and Rh-Ir-ReO_x/SiO_2 after the reduction. (I) Re L_3-edge XANES spectra, (II) Relation between white line area and valence of Re. (a) Re powder, (b) Ir-ReO_x/SiO_2 after glycerol hydrogenolysis[44], (c) Rh(0.66)-Ir-ReO_x/SiO_2, (d) Rh(1)-Ir-ReO_x/SiO_2, (e) Rh(2)-Ir-ReO_x/SiO_2 after the reduction, (f) ReO_2, (g) ReO_3 and (h) Re_2O_7.

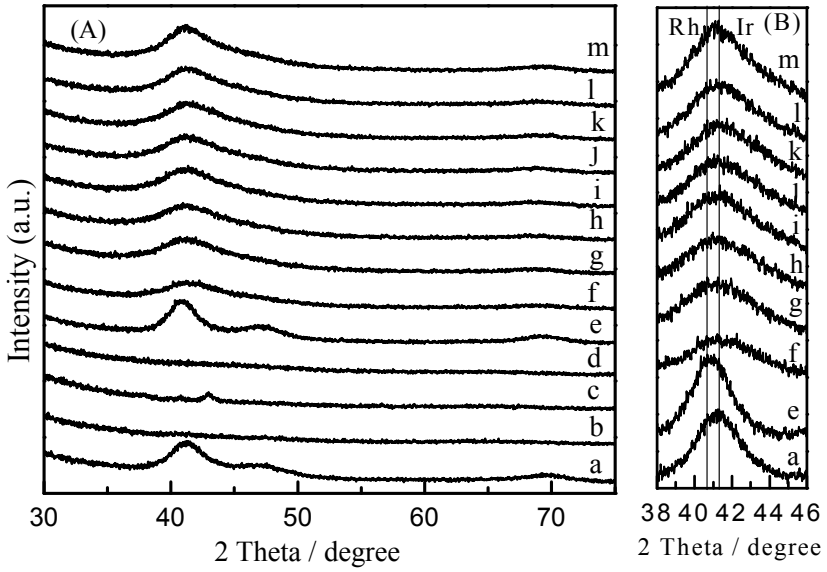

Fig. 4. XRD patterns of catalysts. (a) Ir/SiO_2 (Ir=4 wt%), (b) Rh/SiO_2 (Rh=0.66 wt%), (c) ReO_x/SiO_2 (Re=7.8 wt%), (d) $Rh\text{-}ReO_x/SiO_2$ (Rh=0.66 wt%, Re=7.8 wt%), (e) $Rh\text{-}Ir/SiO_2$ (Rh=0.66 wt%, Ir=4 wt%), (f) $Ir\text{-}ReO_x/SiO_2$ (Ir=4 wt%, Re/Ir=2) after reduction at 473 K for 1 h. (g) $Rh(0.1)\text{-}Ir\text{-}ReO_x/SiO_2$, (h) $Rh(0.3)\text{-}Ir\text{-}ReO_x/SiO_2$, (i) $Rh(0.5)\text{-}Ir\text{-}ReO_x/SiO_2$, (j) $Rh(0.66)\text{-}Ir\text{-}ReO_x/SiO_2$, (k) $Rh(0.75)\text{-}Ir\text{-}ReO_x/SiO_2$, (l) $Rh(1)\text{-}Ir\text{-}ReO_x/SiO_2$ and (m) $Rh(2)\text{-}Ir\text{-}ReO_x/SiO_2$ after reaction. (A) 2 theta range 30-75°, (B) 2 theta range 38-46°, intensity × 4.

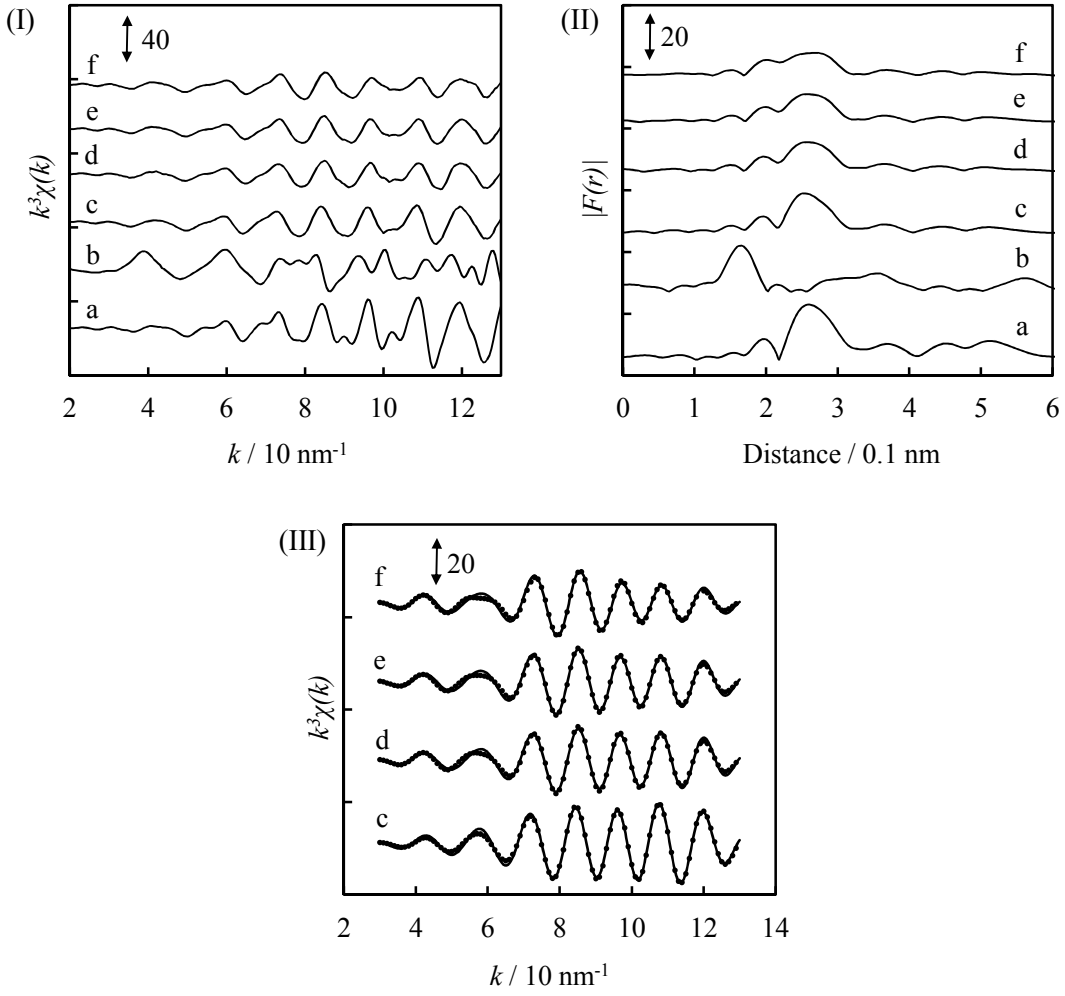

Fig. 5. Results of Ir L_3-edge EXAFS analysis of Ir-ReO_x/SiO_2 and Rh-Ir-ReO_x/SiO_2 after the reduction. (I) k^3-Weighted EXAFS oscillations. (II) Fourier transform of k^3-weighted Ir L_3-edge EXAFS, FT range: 30–130nm^{-1}. (III) Fourier filtered EXAFS data (solid line) and calculated data (dotted line), Fourier filtering range: 0.163-0.325 nm. (a) Ir powder, (b) IrO_2, (c) Ir-ReO_x/SiO_2 after glycerol hydrogenolysis[44] and (d-f) Rh−Ir−ReO_x/SiO_2 after the reduction ((d) Rh = 0.66 wt%, (e) Rh =1 wt% and (f) Rh = 2 wt%).

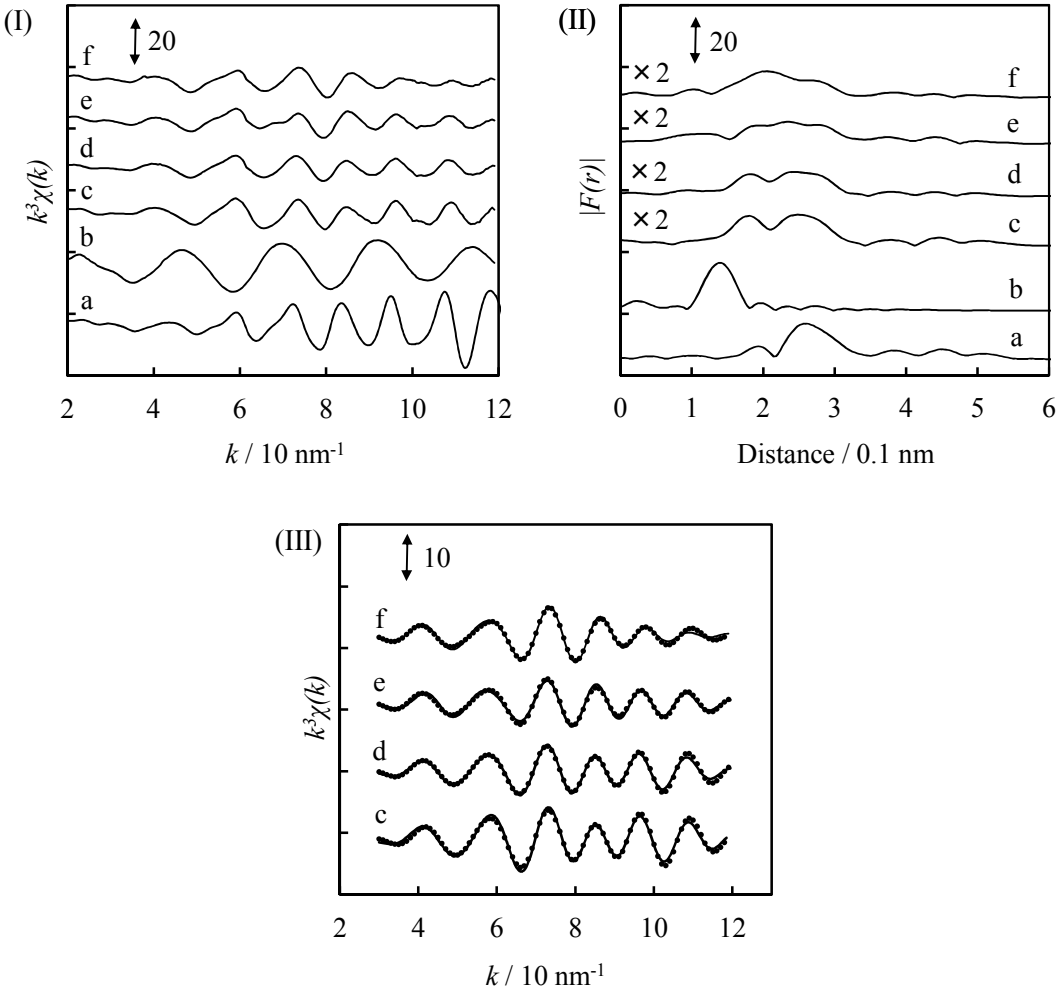

Fig. 6. Results of Re L_3-edge EXAFS analysis of Ir-ReO_x/SiO_2 and Rh-Ir-ReO_x/SiO_2 after the reduction. (I) k^3-Weighted EXAFS oscillations. (II) Fourier transform of k^3-weighted Re L_3-edge EXAFS, FT range: 30–120 nm^{-1}. (III) Fourier filtered EXAFS data (solid line) and calculated data (dotted line), Fourier filtering range: 0.138–0.325 nm. (a) Re powder, (b) NH_4ReO_4, (c) Ir-ReO_x/SiO_2 after glycerol hydrogenolysis[44] and (d-f) Rh-Ir-ReO_x/SiO_2 after the reduction ((d) Rh = 0.66 wt%, (e) Rh =1 wt% and (f) Rh = 2 wt%).

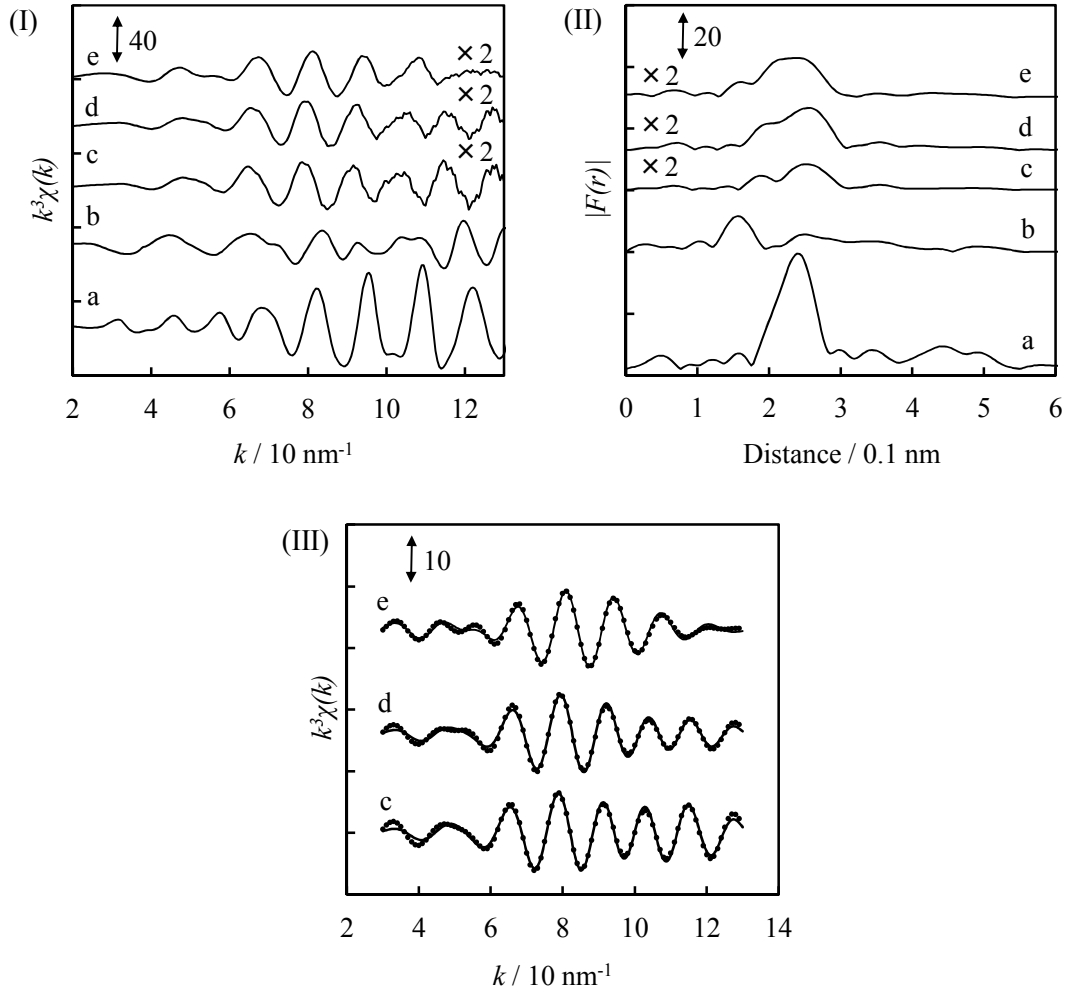

Fig. 7. Results of Rh *K*-edge EXAFS analysis of Rh-Ir-ReO_x/SiO_2 after the reduction.
(I) k^3-Weighted EXAFS oscillations. (II) Fourier transform of k^3-weighted Rh *K*-edge EXAFS, FT range: 30-130 nm^{-1}. (III) Fourier filtered EXAFS data (solid line) and calculated data (dotted line), Fourier filtering range: 0.163-0.310 nm. (a) Rh foil, (b) Rh_2O_3, (c-e) Rh-Ir-ReO_x/SiO_2 after the reduction ((c) Rh = 0.66 wt%, (d) Rh =1 wt% and (e) Rh = 2 wt%) .

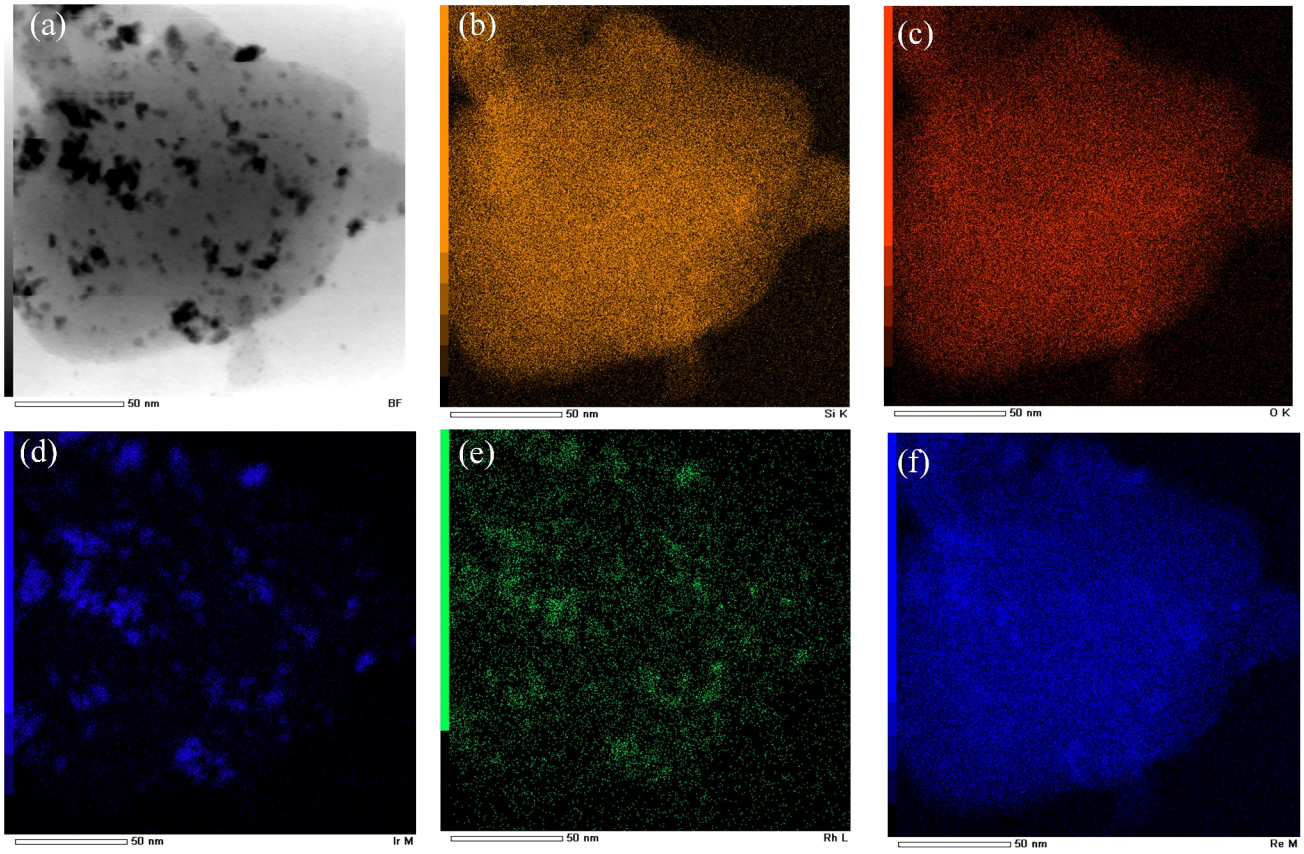

Fig. 8. TEM image and STEM-EDX mappings of Rh(0.66)-Ir-ReO_x/SiO_2 after reduction. The maps reflect the measured (b) Si K intensity, (c) O K intensity, (d) Ir M intensity, (e) Rh L intensity, (f) Re M intensity.

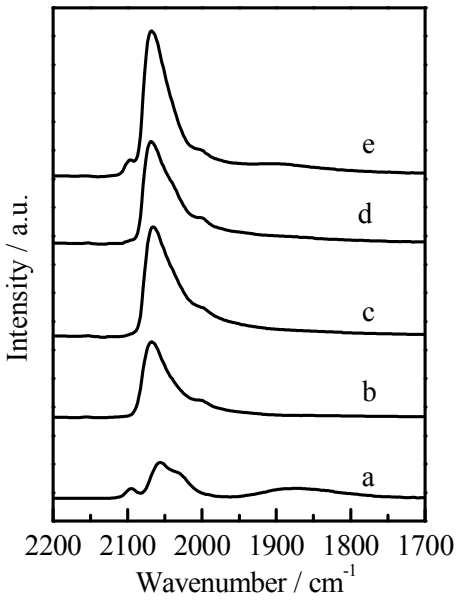

Fig. 9. DRIFT spectra of CO adsorbed on the catalysts after reduction at 473 K. (a) Rh/SiO_2 (Rh=0.66 wt%), (b) Ir-ReO_x/SiO_2 (Ir=4 wt%, Re/Ir=2), (c) Rh(0.66)-Ir-ReO_x/SiO_2, (d) Rh(1)-Ir-ReO_x/SiO_2 and (e) Rh(2)-Ir-ReO_x/SiO_2.